CHEMICAL REVIEWS

Volume 99, Number 3 March 1999

Transition-Metal Ions in Aluminophosphate and Silicoaluminophosphate Molecular Sieves: Location, Interaction with Adsorbates and Catalytic Properties

Martin Hartmann

Institute of Chemical Technology I, University of Stuttgart, D-70550 Stuttgart, Germany

Larry Kevan*

Department of Chemistry, University of Houston, Houston, Texas 77204-5641

Received January 21, 1997 (Revised Manuscript Received November 19, 1998)

Contents

Martin Hartmann received his Ph.D. at the University of Dortmund involving multinuclear nuclear magnetic resonance studies on copper ions in faujasites. He then spent two years as a postdoctoral research associate at the University of Houston studying electron spin–echo spectrometry of metal ions in microporous materials. He has presented his work at several internal conferences. Currently he has a fellowship to work toward his habilitation certification at the University of Stuttgart with emphasis on catalytic studies of metal ions in microporous materials.

I. Introduction

Aluminophosphate (AlPO-*n*) and silicoaluminophosphate (SAPO-*n*) molecular sieves, where *n* denotes a particular structure type, form a new class of microporous crystalline materials comparable to the well-known zeolites, which are aluminosilicate molecular sieves. Zeolites have pores or channels formed by alumina and silica tetrahedra linked by oxygen bridges. Substitution of other elements for Al and/or Si in the molecular sieve framework can yield various kinds of new materials. Wilson et al. reported in 1982 the synthesis of aluminophosphate molecular sieves.[1] The structures of AlPO and SAPO molecular sieves cover a wide range of different structure types; some are analogous to certain zeolites such as SAPO-42 (A zeolite structure), SAPO-34 (chabazite struc-

10.1021/cr9600971 CCC: $35.00
Published on Web 02/10/1999

Larry Kevan received his Ph.D. at the University of California at Los Angeles. He has taught at the University of Chicago, University of Kansas, Wayne State University, and University of Houston where he is the Cullen Distinguished Professor of Chemistry. His research interests focus on the development and applications of electron magnetic resonance methods, especially pulsed electron spin echo methods, to disordered media and microporous materials.

ture), or SAPO-37 (faujasite structure). But there is also a large number of aluminophosphates such as AlPO-5, AlPO-11, or VPI-5, which are unique structures with no zeolite analogue.[2] An exciting property of the AlPO-*n* materials is that Al and/or P can be replaced by silicon to form SAPO-*n* materials and often by other metals to form MeAPO-*n* or MeAPSO-*n* materials.[3−5] The numbering of the structure types of SAPO-*n*, MeAPO-*n* or MeAPSO-*n* follows that of AlPO-*n*, so that SAPO-5 denotes the same structure type as AlPO-5. Initially, Flanigen et al.[5] reported the incorporation of 13 elements into AlPO-5, including the transition metal ions titanium, manganese, iron, cobalt, and zinc. It has been claimed that a variety of metals can be incorporated into the aluminophosphate structure (Figure 1), but actual incorporation into the tetrahedral framework is difficult to prove.

The major structures in the AlPO-*n* and SAPO-*n* molecular sieves are shown in Table 1. Beside fifteen novel structures, seven structures with framework topologies related to aluminosilicates (zeolites): chabazite (n = 34, 44, 47), erionite (17), faujasite (37), gismondine (43), levynite (35), Linde Type A (42), and sodalite (20) were discovered. Most studies have dealt with structure types AFI (AlPO-5), AEL (AlPO-11), or CHA (AlPO-34), but numerous other structures (ATS, AFO, VFI, etc.) will also be discussed in this review.

The AlPO-5 molecular sieve is composed of 4-ring, 6-ring, and 12-ring straight channels which are interconnected by 6-ring windows. The main channels of this structure type are nearly circular and have a diameter of 0.73 nm. In AlPO-11 the main channels are formed from 10-rings with an elliptical shape of 0.63 by 0.39 nm. Structure type 34 has the chabazite zeolite structure with ellipsoidal cages which can be accessed through 8-ring windows with 0.38 nm diameter. Replacement of some phosphorus by silicon in neutral framework AlPO materials produces SAPO materials with a negative framework charge. These framework charges are balanced by H^+ after template removal by calcination. The H^+ ions can be exchanged to some extent by transition metal ions, and the ion-exchanged products are denoted as MeH-SAPO-*n* with a dash between the metal type and the SAPO designation.

The incorporation of transition metal ions into framework sites of the aluminophosphate and silicoaluminophosphate molecular sieves is also of particular interest for the design of novel catalysts. Paramagnetic metal species are often introduced into molecular sieves to generate a catalytically reactive species or site. Various pretreatment or activation procedures are typically used to generate reactive metal ion valence states which are often paramagnetic. The location and structure of the reactive metal ion site is of considerable importance for understanding the chemistry of such materials. In particular, the interaction of such active metal ion sites with different adsorbates and reactants helps to understand catalysis on a molecular level. A sufficiently good understanding of the local adsorbate structure of catalytically active metal species in microporous materials can potentially enable optimization and control of the catalytic activity of such systems.

Transition metal ions can be incorporated by three different methods: inpregnation, ion-exchange, and isomorphous substitution. In the latter method the transition metal ion salt is incorporated directly into the synthesis mixture. Since the comprehensive paper of Flanigan,[4] "Aluminophosphates and the periodic table," many studies have been published, claiming the isomorphous substitution of transition metal ions into the framework of different structure types.

Information on cation location or the incorporation of transition metal ions into aluminophosphates and silicoaluminophosphates is typically hard to obtain since the metal concentration is very low. A large number of different characterization methods have been used to collect information on the location of the transition-metal ion in the molecular sieve. Conclusive judgments can usually only be made by using complementary techniques for characterization of the same samples.

The locations of charge-balancing cations are important to understand the catalytic and adsorptive properties of molecular sieves. Possible cation locations in SAPO-11 are close to the walls of the channels adjacent to 6-rings because the 4-, 6-, and 10-rings are interconnected by 6-ring windows. Also there are possible cation sites that are recessed into the 10-ring channels, because the 10-rings have an elliptical cross section. By analogy to cation sites in zeolites X and Y, Lee et al.[6] proposed possible sites in H-SAPO-11 as follows (see Figure 2a). Site U is at the center of the double 10-ring channel. Site I is at the center of the double 6-rings that form 6-ring channels. Site I′ is in the plane of the O_3 oxygens of the 6-ring. Site II is at the center of the hexagonal window on the surface of the 10-ring channels. When we carefully examine the surface of the 10-ring elliptical channel, which is composed of five 6-ring windows, we realize that there are two different kinds of S II sites, i.e., S II_1 and S II_2. Sites II_1 and II_2 have different environments. Site II_1 is located at

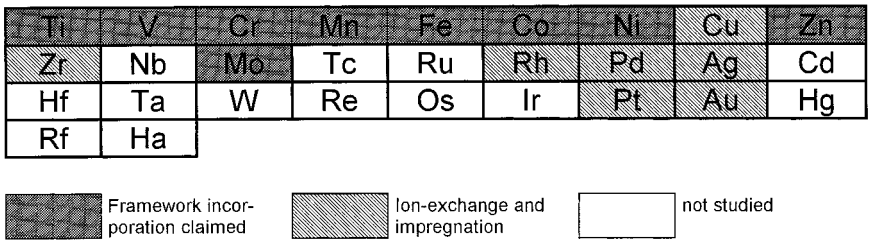

Figure 1. Partial periodic table with transition elements marked which have been introduced into aluminophosphates and silicoaluminophosphates.

Table 1. Structures of AlPO-*n* Molecular Sieves

n	IZA[a] structure code	pore diameter/nm (ring)
	Large Pore	
5	AFI	0.73 (12)
36	ATS	0.75 × 0.65 (12)
37	FAU	0.74 (12)
40	AFR	0.43 × 0.70 (10)
46	AFS	0.64 × 0.62 (12)
		0.4 (8)
	Intermediate Pore	
11	AEL	0.63 × 0.39 (10)
31	ATO	0.54 (12)
41	AFO	0.43 × 0.70 (10)
	Small Pore	
14		
17	ERI	0.36 × 0.51 (8)
18	AEI	0.38 (8)
26		
33	ATT	0.42 × 0.46 (10)
34	CHA	0.38 (8)
35	LEV	0.36 × 0.48 (8)
39	ATN	0.4 (8)
42	LTA	0.41 (8)
43	GIS	0.31 × 0.45 (8)
44	CHA	0.38 (8)
47	CHA	0.38 (8)
	Very Small Pore	
16	AST	(6)
20	SOD	(6)
25	ATV	0.30 × 0.49 (8)
28		
	Very Large Pore	
8	AET	0.79 × 0.87 (14)
VPI-5	VFI	1.21 (18)

[a] International Zeolite Association.

a more recessed position relative to site II_2. Sites II′ and II* correspond to displacement from site II in to and out of the 10-ring channel, respectively (see Figure 2a). The possible cation sites in H-SAPO-5 are analogous except that there is only one type of S II site due to the 12-ring structure (Figure 2b).

The cation sites in H-SAPO-34 can be described by analogy to cation sites in chabazite, which has a similar structure. The framework of SAPO-34 consists of distorted hexagonal prisms linked together by four-membered rings to form a large ellipsoidal cavity. Each ellipsoidal cavity is interconnected to six like cavities through an eight-membered oxygen ring with an opening diameter of about 0.4 nm (Figure 3). Although no X-ray crystallographic data are available on the sites occupied by charge-compensating cations in SAPO-34, an estimate of probable locations can be made from those sites previously determined in the structural analogue mineral chabazite. The designations of these sites are given by Calligaris et al.[7] Site I is displaced from the 6-ring into the ellipsoidal cavity; site II is located near the center of the ellipsoidal cavity; site III is found in the center of the hexagonal prism and site IV is near the 8-ring window (Figure 3).

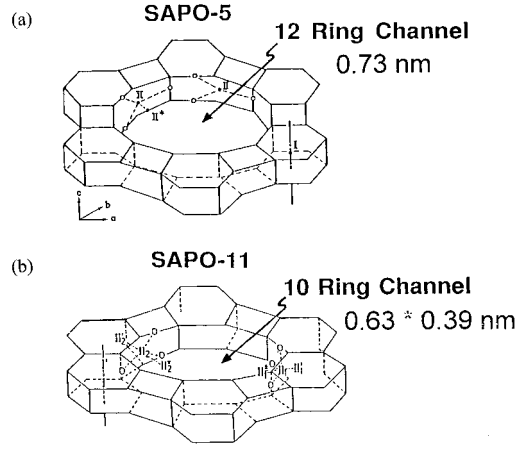

Figure 2. Simplified structures of (a) SAPO-11 and (b) SAPO-5. Each intersection of the lines corresponds to a P, Al, or Si atom with oxygens halfway between. The roman numerals describe cation positions according to the text.

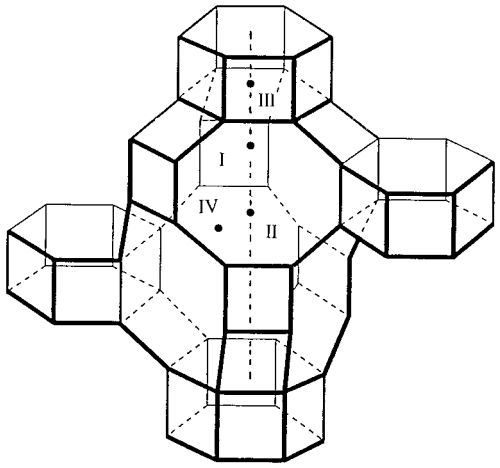

Figure 3. Structure of SAPO-34 illustrating the ellipsoidal cavity. In this representation the vertexes represent either phosphorus, aluminum, or silicon atoms and the lines connecting the vertexes represent oxygen bridges. The roman numerals indicate cation sites.

Scope of the Review. A prerequisite for understanding the catalytic properties of transition metal containing aluminophosphates and silicoaluminophosphates is a thorough characterization of the transition metal ion environment. Therefore, studies on the location and interaction of these ions with different

adsorbates are reviewed in detail. Some catalytic investigations are summarized in Section III if they are restricted to one particular transition metal ion or help to characterize the material. Three important groups of reactions viz. oligomerizations, oxidations, and methanol to olefin (MTO) conversion are treated in Section IV. It will be shown that (1) a range of complementary techniques (DRS, IR, XPS, ESR, NMR, EXAFS etc.) is necessary to unravel the environment of the transition metal ion, (2) it is possible to control the location and the oxidation state of the transition metal ion, and (3) transition metal ion containing AlPOs and SAPOs are promising materials for catalytic applications.

II. Characterization Methods

The catalytic properties of microporous materials are largely determined by the composition and structure on the atomic scale. Therefore, catalyst characterization is a lively and highly relevant discipline in catalysis. A large variety of different characterization methods have been applied depending on the nature and the valence state of the transition metal ion. Information on cation location in silicoaluminophosphates is typically hard to obtain since the metal concentration is very low. Therefore X-ray diffraction (XRD), which has been employed in zeolites to determine cation locations, cannot typically be used. Infrared (IR) and diffuse reflectance infrared Fourier transform (DRIFT) spectroscopy have been applied sucessfully as well as Raman spectroscopy.[8] Infrared and nuclear magnetic resonance (NMR) spectroscopy as well as other techniques can be used to study the catalyst in situ under working conditions. This has been shown most successfully with IR and NMR for aluminosilicates (zeolites).[9] In situ methods are only beginning to be applied to microporous aluminophosphates and silicoaluminophosphates.

Electron spin resonance (ESR) and a pulsed ESR method known as electron spin−echo modulation (ESEM) have become powerful tools for analyzing catalytically important oxide systems containing paramagnetic ions.[10−14] The ESEM method is particularly well adapted for studying powder spectra in molecular sieves. Paramagnetic species can be located with respect to various surface or framework atoms by analyzing the ESE modulation signal, which is associated with very weak electron−nuclear dipolar hyperfine interactions with surrounding magnetic nuclei to distances of about 0.6 nm. By using deuterated or ^{13}C-labeled adsorbates it is possible to determine the number of adsorbed molecules and their distance to a catalytically active center. Ordinary electron spin resonance spectrometry normally does not allow such detailed structural information to be obtained.

Several other techniques including Mössbauer spectroscopy, X-ray photoelectron spectroscopy (XPS), and EXAFS (extended X-ray absorption fine structure) have been used in fewer cases. EXAFS provides a description of the short-range order of selected atomic species in terms of the number of neighbors, distances, and thermal and static disorder within the range of those distances. The technique is based on the absorption of X-rays and the creation of photoelectrons which are scattered by nearby atoms in the lattice. Mössbauer spectroscopy is relatively little used in catalyst characterization since it is limited to those elements that exhibit the Mössbauer effect. Iron, tin, iridium, ruthenium, and platinum are the relevant Mössbauer metals for introduction into AlPO-*n* and SAPO-*n* materials. Mössbauer spectroscopy provides valuable information on oxidation states, magnetic fields, lattice symmetry, and lattice vibrations.

X-ray photoemission electron spectroscopy is a widely used method for surface chemical analysis. It yields information on the elemental composition, the oxidation state of the element, and in favorable cases on the dispersion of one phase over another. The technique was initially named electron spectroscopy for chemical analysis (ESCA), but the acronym XPS is now more common.

UV−vis spectroscopy is commonly employed for the characterization of chromium-, cobalt-, titanium-, or vanadium-containing samples. UV−vis spectra of powder samples are typically recorded in the diffuse reflectance mode and labeled DRS spectra (not to be confused with DRIFT spectra).

III. Characterization and Location of Transition Metal Ions

A. Titanium

After the discovery of titanium-substituted silicalite-1 (TS-1) with its remarkable catalytic properties, particularly for oxidation reactions under mild conditions, titanium incorporation has been tried in other materials as well. Titanium substitution has been claimed in the frameworks of SAPO-5,[15,16] AlPO-5,[21] AlPO-11,[17] and $AlPO_4$-36.[18,19] While titanium replaces silicon in large silica patches of SAPO-5,[15] Ti substitution in pure AlPO-*n*, leading to Ti−O−P bonds,[20] is expected to be more difficult.[17]

UV−vis spectra of titanium-containing samples showed a single line centered near 230 nm indicating tetrahedral Ti^{4+}. The absence of a shoulder near 300 nm suggests that anatase-like phases were not formed during the synthesis of titanium-containing aluminophosphates and silicoaluminophosphates.[19]

Samples with incorporated titanium also showed an IR band at 970 cm^{-1}. This band has been taken as evidence for the presence of Ti^{4+} ions in tetrahedral coordination and can be attributed to SiO^- defects in the silica patches indicating the substitution of Ti^{4+} for Si^{4+} in the SiO_2 domains.[16,21] A shoulder at 1040 cm^{-1} in the IR spectrum of calcined TAPO-*n* is assigned to the presence of titanium in the framework.[15]

Evidence for the isomorphous substitution of titanium into aluminophosphates with the AFI structure is reported by combined use of ESR and ESEM spectroscopy by comparing synthesized TAPO-5 and TiO_2/SAPO-5.[22] γ-Irradiation and CO reduction are both effective in producing paramagnetic Ti(III) species in TAPO-5, while γ-irradiation also produces a hole center on oxygen called a V center. An ESR signal with a rhombic **g** tensor ($g_1 = 1.965$, $g_2 = 1.92$,

Table 2. ESR Parameters of V(IV) Containing AlPO Molecular Sieves and Selected Related Systems

sample	*T*/K	species	g_{xx}	g_{yy}	g_{zz}	A_{xx}[a]	A_{yy}[a]	A_{zz}[a]	ref
VAPO-5	120	A	1.977	1.993	1.947	7.42	7.42	19.6	34
		B	1.975	1.992	1.930	7.4	7.4	19.5	34
VAPO-5	77		1.99	1.99	1.937	8.0	8.0	19.5	36
VAPO-5	77	A	1.983	1.983	1.932	7.3	7.3	19.8	27
		B	1.983	1.983	1.935	7.3	7.3	19.3	27
VAPO-5	77		2.000	2.000	1.940	7.3	7.3	19.3	24
VAPO-5	300	A	1.975	1.975	1.934	6.6	6.6	17.7	26
		B	1.975	1.975	1.927	6.6	6.6	17.5	26
VAPSO-5	293	A′	1.976	1.976	1.935	7.1	7.1	19.6	35
		B′	1.978	1.978	1.930	7.3	7.3	19.6	35
VAPO-31			1.987	1.987	1.932	8.0	8.0	19.9	29
V_2O_5/AlPO-5	300	A	1.975	1.975	1.935	6.6	6.6	17.7	26
		B	1.988	1.988	1.988				26
VS-1 tetrahedral V	77		1.912	1.912	1.912	3.5	3.5	19.1	254
V_2O_5/ZSM-5 vacuum treated	300		1.990	1.990	1.928	8.1	8.1	20.6	255
VO^{2+}/ZSM-5 hydrated	300		1.990	1.990	1.949	7.3	7.3	18.6	256
V^{4+}/ThGeO4	77		1.980	1.980	1.831	3.5	3.5	19.1	257
V/MCM-41	293	A″	1.981	1.981	1.936	6.9	6.9	18.9	259
		B″	1.981	1.981	1.945	6.9	6.9	19.1	259

[a] Given in mT.

and $g_3 = 1.879$) is assigned to trivalent titanium in a framework site. The γ-irradiation of TiO_2/SAPO-5 gives an ESR signal typical of Ti(III) with octahedral symmetry ($g_{||} = 1.971$ and $g_{\perp} = 1.907$), which is also found after CO reduction. CO reduction of TAPO-5 also gives an ESR signal with a rhombic **g** tensor, which is different from that for Ti(III) formed by γ-irradiation. These differences are due to additional coordination of tetrahedral framework titanium with CO molecules. Simulation of the ^{31}P ESEM spectra for Ti(III) ions in TAPO-5 shows one phosphorus atom at 0.39 nm and two phosphorus atoms at 0.48 nm, which is consistent with titanium substitution for framework phosphorus.

B. Vanadium

There is a large interest in vanadium analogues of molecular sieves based on zeolites and aluminophosphates mainly based on their potential to catalyze oxidation reactions. The incorporation of vanadium into silicalite[23] and AlPO-*n*[4] has been reported. However, successful incorporation of vanadium into the framework of aluminophosphates is still controversial. Therefore, several spectroscopic techniques have been used to investigate vanadium species in AlPOs and SAPOs.

There are several reports on vanadium containing aluminophosphate molecular sieves using ESR spectroscopy for the detection of V(IV) in VAPSO- and VAPO-5, -11, -31, -37, -40, and -41 and VPI-5.[24−33] The ESR of these samples shows well resolved hyperfine splittings corresponding to V(IV) cations bonded strongly to oxygen ions in the matrix (Table 2). The V(IV) ESR parameters for as-synthesized VAPO-5 are about $g_{||} = 1.93$, $A_{||} = 190$ G, $g_{\perp} = 1.98$ and $A_{\perp} = 72$ G per Table 2. Whittington et al.[26] and Montes et al.[27] find two different V(IV) species with very similar **g** tensor parameters. One of these species is also found in a V_2O_5 impregnated AlPO-5 in which a single line at $g = 1.988$ is detected. This line is also found in pure V_2O_5. VAPO-5 with seven well-resolved hyperfine lines is ascribed to isolated vanadyl-like V(IV) ($I = 7/2$) species. After calcination of VAPO-5 in flowing oxygen at 500 °C the signal intensity decreases by 40-fold,[24] which is ascribed to the oxidation of the vanadyl-like species toV^{5+} according to the reaction in eq 1.

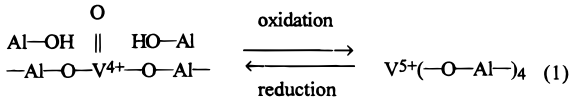

(1)

The signal intensity can be increased by hydrogen reduction or high-temperature exposure to organic molecules such as toluene or *p*-xylene. The reported results mainly underline the redox properties of vanadium in aluminophosphates and do not discuss the ESR parameters in terms of demonstrating possible framework incorporation of V^{4+}. More recent ESR results by Weckhuysen et al.[34] and Lohse et al.[35] found no unambiguous evidence for true incorporation of V(IV) into tetrahedrally coordinated framework positions of VAPO-5, VAPSO-5, and VAPSO-44. In as-synthesized samples two signals with similiar **g** tensor parameters (Table 2) are ascribed by Weckhuysen et al. to isolated (pseudo-) octahedral V(IV). Very similiar **g** tensor parameters are ascribed by Lohse et al. to isolated immobile VO^{2+} species in square-pyramidal symmetry.[35] Upon calcination, V(IV) ions are oxidized to tetrahedral V(V) which can only be partially reduced to V(IV). However, the ESR detectable vanadium content is below 20% of the total vanadium.

The diffuse reflectance spectra (DRS) of reference compounds such as V_2O_5, NH_4VO_3, and vanadium supported on Mg were compared with VAPO-5 samples of different vanadium content.[34] A band around 270−290 nm is assigned to isolated tetrahedral V(V) sites supporting the incorporation of vanadium into the framework. A broad band is observed in the 350−450 nm region suggesting that some polymeric vanadium species, probably V_2O_5-like, are present. AlPO-5 samples impregnated with vanadium show only slightly different DR spectra. These spectra also give peaks at 290 nm, suggesting a tetrahedral environment for V(V), and around 410

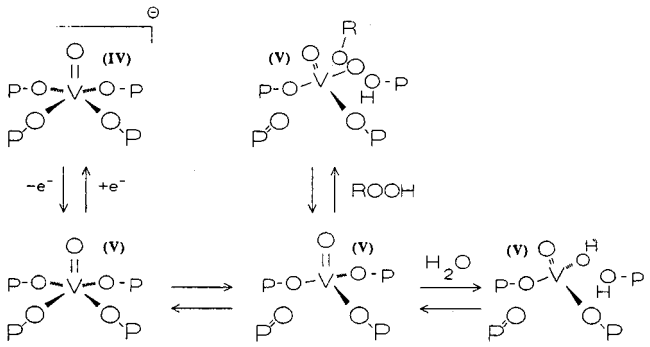

Figure 4. Possible structure of the vanadium species in VAPO-5 and its reaction with water and ROOH.

nm, which is ascribed by Blasco et al.[36] to polymeric forms of vanadium like in V_2O_5.

Solid-state ^{51}V NMR studies on V-containing catalysts[25] have shown that it is possible to obtain information on the symmetry environment of ^{51}V by comparison with model compounds. The ^{51}V NMR spectra have been taken under static and magic angle spinning (MAS) conditions.[25] The ^{51}V isotope has a moderately large electric quadrupole moment, and the line shape of the wide line spectra is dominated by chemical shift anisotropy rather than by second-order quadrupolar effects. The wide-line ^{51}V NMR spectra are mainly formed by a broad signal with a maximum slightly upfield from −300 ppm (reference $VOCl_3$). ^{51}V MAS NMR spectra of calcined VAPSO-11 show a narrow chemical shift distribution with an isotropic shift $\sigma_{iso} = -540$ ppm. The ^{51}V MAS NMR pattern is consistent with previously published literature of predicted square pyramidal or distorted octahedral vanadyl(V) species in VAPO-5. Similiar ^{51}V MAS NMR spectra were obtained for VAPO-11.[37]

VAPO-5 was found to catalyze oxidation reactions (see Section IV) with *tert*-butyl hydroperoxide (TBHP) such as epoxidation of allylic alcohols (>95% selectivity at 50% conversion of the substrate) and oxidations of aromatic compounds.[26] On the basis of the interaction of vanadium species in VAPO-5 with TBHP and *tert*-butyl alcohol, a model was proposed for the catalytic site (Figure 4). The scheme involves a one-electron redox reaction and several solvolysis equilibria and is consistent with most spectroscopic results.

C. Chromium

In the patent literature[28] the synthesis of CrAPO-5 has been reported, but the remaining question concerns the possibility and the extent of tetrahedral Cr(III) substitution for Al^{3+} in the framework. Isomorphous substitution requires tetrahedral coordination of Cr(III), which is very rare in inorganic complexes because the crystal field stabilization energy of octahedral Cr(III) (224.5 kJ/mol) is much greater than that for tetrahedral Cr(III) (66.9 kJ/mol).[38,39] Therefore, tetrahedral coordination of Cr(III) in aluminophosphates should be difficult to achieve. Although several papers report the synthesis of chromium-containing AlPOs and their application as advanced materials,[40−43] only limited effort was made to characterize these materials. Only for CrAPO-14, an aluminophosphate with octahedral framework sites, was it shown by single-crystal XRD that 5% of the octahedral sites are occupied by Cr(III).[44] In the papers by Weckhuysen and Schoonheydt,[45,46,47] CrAPO-5 formed by Cr_2O_3 or $Cr(NO_3)_3 \cdot 9H_2O$ added to the synthesis mixture was compared to AlPO-5 impregnated with Cr(III). The ESR signals of the synthesized and impregnated AlPO-5 containing Cr(III) are comparable. A redox cycle Cr(III) → Cr(V) is reported on the basis of DRS and ESR data. During and after hydrothermal synthesis, Cr(III) is in (pseudo-) octahedral coordination with oxygen in CrAPO-5 and CrAPSO-11. This is illustrated by ESR and by DRS spectra displayed in Figure 5. As-synthesized CrAPSO-11 and CrAPO-5 show a broad signal around $g = 2.0$ with a positive lobe between $g = 5$ and 4. In most preparations the signal near $g = 2$ appears with varying intensity as does the positive lobe which position varies between $g = 5$ and 4. This signal has some similarities with the δ-signal on amorphous supports and can be simulated using large zero-field parameters.[48] After calcination and rehydration during cooling, CrAPSO-11 shows a much narrower ESR spectrum, which is assigned to Cr(V), possibly in square-pyramidal coordination.[49] A three-pulse ^{31}P ESEM spectrum was obtained for CrAPSO-11 evacuated at room temperature for 12 h and simulated with 11−12 phosphorus interacting with Cr(V) at a distance of 0.58 nm. The three-pulse ESE for solid-state ion-exchanged Cr−SAPO-11 does not show any ^{31}P modulation. Although there are some additional hints for isomorphous substitution of Cr(III) in SAPO-11, there are still some unclear aspects which are beyond the scope of this review. Wechhuysen et al.[47] concluded on the basis of their X-band, Q-band, and DRS data that Cr(III) is not incorporated into the framework, but is present as octahedral ions at the surface of the AlPO-5 crystals. Analogous results were obtained by Rajic et al.[50] in the CrAPSO-34-system, where Cr also is believed to be an extraframework species. The adsorption maxima for as-synthesized CrAPSO-34 and calcined CrAPSO-34 are 420, 575, 666, and 370 nm, respectively. The

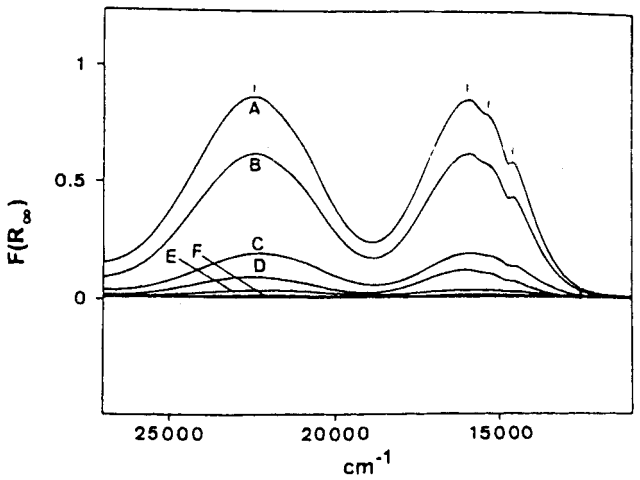

Figure 5. DRS spectra of as-synthesized CrAPO-5 with increasing Cr content: $0.75\ Et_3N \cdot (Cr_xAl_yP)O_4 \cdot 20H_2O$ with $x = 0.08$ (A); 0.04 (B); 0.02 (C); 0.004 (D); 0.002 (E); and 0 (F). (Reprinted with permission from ref 45. Copyright 1994 Elsevier.)

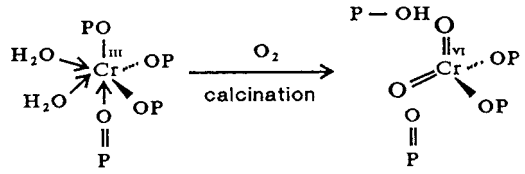

Figure 6. Location of chromium in as-synthesized and calcined CrAPO-5.

spectrum of as-synthesized CrAPSO-34 indicates the presence of octahedrally coordinated Cr(III), which is oxidized to Cr(VI) and the UV−vis spectrum of the calcined material corresponds to the chromate ion, CrO_4^{2-}.

Large CrAPO-5 crystals have been characterized by single-crystal UV−vis spectroscopy, and a polarization dependent absorption has been observed.[43] The $^4T_1$ band has its maximum at 454 nm for the polarization parallel to the pores and at 445 nm for polarization perpendicular to them. The $^4T_2$ band is 625 ± 15 nm for both polarizations. This indicates an aniostropic coordination of Cr(III) distorted by the molecular sieve structure. However, the band positions point to a 6-fold coordination, which is a strong argument against isomorphous substitution in the framework.

Isomorphous substitution of Cr(III) into framework sites of CrAPO-11 was reported by Eswaramoorthy et al.[51] As-synthesized and calcined CrAPO-11 show *no* peak in the ESR spectra, which was taken by the authors as evidence for tetrahedral Cr(III) in their sample.[52]

Distinct differences between the CrAPSO-11 system and the supported Cr/SAPO-11 catalyst were observed by the combined use of UV−vis, XPS, and IR spectroscopy[38] and linked to the catalytic performance of these two systems for the isomerization of 1-butene. On oxidized CrAPSO-11 a large fraction of Cr(VI) was found by UV−vis and XPS, which showed that almost 70% of the chromium existed as Cr(VI). For oxidized Cr/SAPO-11 82% of the Cr was Cr(III). These results are supported by IR spectroscopy employing NO as a probe. The NO chemisorption experiments showed the presence of high chromium oxidation states in oxidized CrAPSO-11, while no evidence of these states was observed for Cr/SAPO-11. After reduction, the distribution of oxidation states on CrAPSO-11 was about 40% Cr(VI) and 60% Cr(IV). In contrast, no differences between oxidized and reduced Cr/SAPO-11 were observed.

Incorporation of chromium(III) into the SAPO-37 framework was investigated by Spinacé et al.[53] The UV−vis spectrum shows two bands at 420 and 620 nm, which are assigned to d−d transitions of Cr(III) in octahedral coordination indicative of an extraframework species. The ESR spectrum of as-synthesized CrAPSO-37 is analogous to the spectra of CrAPO-5 and CrAPSO-11 and shows a broad peak at $g = 1.98$ and an absorption at $g = 4$.

In light of their data on CrAPO-5, Chen and Sheldon[54] put forward a model, which explains the increase in acidity in their system (Figure 6). They assumed that in as-synthesized CrAPO-5, Cr(III) is octahedrally coordinated within the framework but with two water ligands. During calcination Cr(VI) is formed, which is still in the AlPO-5 structure (Figure 6). To balance the charges, Cr(VI)AlPO-5 must contain an acidic P−OH. By using acetonitrile, the authors confirmed the presence of strong Lewis acid sites and acidic P−OH groups in CrAPO-5.

Peeters et al.[55] reported a quantitative ^{31}P MAS NMR study of CrAPO-11. They found that substitution of Cr had a significant effect on the framework, in which at least the phosphorus in the first and third coordination spheres around Cr became NMR invisible. In contrast, nonframework chromium does not have such an effect.

Although some data suggest the incorporation of chromium into the molecular sieve framework of AlPO-11, AlPO-5, or the analogous silicoaluminophosphates, this controversial issue is not settled. Some authors found in CrAPSO-34[50] and CrAPO-5[45−47] that Cr(III) is not incorporated into the molecular sieve framework during synthesis. Other studies[38,49,54] suggested the incorporation of tetrahedral Cr(VI) while another has stressed the significant effect that the substitution of Al by Cr has on the framework.[55]

D. Manganese

Manganese is commonly accepted as a possible candidate for isomorphous substitution into microporous aluminophosphates.[56] Mn(II) incorporation into the framework of AlPO-*n* and SAPO-*n* ($n = 5$, 11) was studied by ESR methods in several papers.[57−65] Goldfarb et al.[57,58] concluded that the majority of Mn(II) in MnAPO-5 does not occupy a framework site, while Brouet et al.[59,62] reported direct ESEM evidence for Mn substitution into a framework position of MnAPO-11 and MnAPSO-11. Pluth et al.[64] showed that Mn(II) is tetrahedrally coordinated in framework positions of as-synthesized MnAPO-11 by single-crystal X-ray diffraction.

The ESR spectrum of MnAPO-5 with a low manganese content shows six resolved hyperfine lines with a splitting often considered typical of octahedral Mn(II) ($I = 5/2$), supporting the existence of extraframework manganese(II).[58,59] On dehydration the spectrum of MnAPO-5 coalesces into a single line. This can also be seen in fresh samples having a higher manganese concentration. The coalescence is attributed to an increase in the spin-exchange interaction due to migration of extraframework Mn(II) within the framework.[59] X-band and Q-band ESR spectra reveal that the spectra seem to be superimposed with a broad signal. Levi et al.[58] assign the origin of this background signal to transitions other than $-1/2 \rightarrow 1/2$ of Mn(II) with $I = 5/2$ and a possible additional Mn(II) species. Removal of water at increasing temperatures up to 400 °C significantly broadens the hyperfine line, and finally at 400 °C the resolution is completely lost and only a broad line is detected. This loss of the hyperfine structure is not detected in samples with much lower Mn(II) contents. Rehydration usually completely restores the spectrum of the hydrated sample.

At high manganese concentrations (1 mol %) the ESR spectra of MnAPO-11, like those of MnAPO-5, are broad with unresolved hyperfine structure and

Table 3. ESR Parameters of Mn(II) in Different Aluminophosphates and Silicoaluminophosphates

sample	treatment	*g*	hyperfine coupling	ref
MnAPO-11	as-synthesized	2.01	87.7 G	60
	calcined	2.01	93.7	60
	calcined + evacuated 360 °C	2.01	87.6	60
	calcined + *o*-xylene	2.01	86.9	60
	calcined + methanol	2.01	93.6	60
Mn-$AlPO_4$-11	impregnated	2.01	93.5	
MnSAPO-11	exchanged with NaCl	2.00	94.5	61
MnH-SAPO-11	exchanged with NaCl	2.00	94.5	61
Mn-SAPO-5	impregnated		95	57
Mn-$AlPO_4$-5	impregnated		90	58
$MnAlPO_4$-5	as-synthesized		90	58

assigned to predominantly extraframework Mn.[57,58,62] This was also tested by ion-exchange with $CaCl_2$, which removed about 30% of the Mn(II). Lowering the concentration to 0.1 mol % Mn gives ESR spectra of hydrated and calcined MnAPO-11 with well-resolved hyperfine lines. The ESR signal of calcined and hydrated MnAPO-11 is better resolved than that of as-synthesized MnAPO-11. In addition to this resolution enhancement, an increase of the hyperfine splitting from 87.7 to 93.7 G is measured upon calcination and hydration. Dehydration at 330 °C leads again to a decrease to 87.6 G (Table 3). From experiments with samples of different manganese content, it was concluded that similar concentrations in synthesized and impregnated samples exhibit different ESR spectra. The spectra of impregnated Mn/AlPO-11 are less well resolved in comparison to those of as-synthesized MnAPO-11. This indicates that the spin−spin interaction is stronger in some impregnated samples and suggest some aggregation of Mn(II) in impregnated samples. Obviously, the manganese species environments in MnAPO-11 and Mn/AlPO-11 are different, suggesting that Mn(II) is framework substituted in MnAPO-11, since it occupies an extraframework position in Mn/AlPO-11. This framework incorporation is further confirmed from a three-pulse ESEM study of deuterium modulation resulting from interactions of D_2O and partially deuterated methanol with Mn(II). The adsorbate geometry indicates that manganese occupies a negatively charged framework site in MnAPO-11. The best fit in case of water adsorption in MnAPO-11 requires a two-shell model with deuteriums at two different distances. However, an interesting point is that there is a significant difference in the spin−echo patterns between MnAPO-5 and MnAPO-11.[62] The pattern of MnAPO-5 is fit by a one-shell model of four deuterium atoms at a distance of 0.29 nm consistent with solvation of two water molecules around a manganese cation in an extraframework position. The stronger modulation in the impregnated Mn/AlPO-5 shows that Mn is coordinated to six deuteriums, which implies three water molecules. The different parameters for Mn(II) in AlPO-5 and AlPO-11 are compared in Table 4.

The analysis of the ^{31}P modulation should provide more evidence for framework incorporation of manganese. If Mn(II) substitutes for ^{27}Al into the framework, then it should be surrounded by a tetrahedral arrangement of four ^{31}P nuclei in a distance at about 0.31 nm. In contrast, the experimental data indicate a significantly larger interaction distance of 0.5 nm for six P nuclei. In AlPO-5 ESR and ESEM results show the similarities between synthesized and impregnated samples, indicating that framework incorporation of Mn(II) into these samples is not likely. In contrast, framework incorporation of a small amount of manganese can be achieved in MnAPO-11 and MnAPSO-11.[59−62]

Table 4. Simulated ^2D ESEM Data of Manganese(II) with Adsorbed Water in Different SAPO Materials

sample	shell	*N*	*r*/nm	A_{iso}/MHz	ref
MnAPO-5	1	4	0.29	0.20	58
Mn/AlPO-5	1	6	0.29	0.20	58
MnAPO-11	1	2	0.24	0.12	59
	2	2	0.36	0.00	59
MnAPSO-11	1	2	0.25	0.24	61
	2	2	0.34	0.01	61

The redox behavior of manganese cations in MnAPO-5 has been investigated by Katzmarzyk et al.[63] Upon calcination in flowing dry oxygen, the color of the material changes from white to violet, while the ESR intensity decreases to one-third of the intensity of the as-synthesized sample. The decrease in signal intensity is attributed by the authors to a partial oxidation of Mn(II) to nondetectable Mn(III). With no other signal appearing even at 93 K, an oxidation to Mn(IV) was ruled out. Reduction of the sample in flowing dry hydrogen at temperatures below 450 K does not change the ESR spectrum, while after reduction at 475 K the ESR signal becomes narrower and more intense. A possible explanation is that reduction of Mn(III) to Mn(II) under these conditions leads to more spins. Rehydration/oxidation cycles are reversible as are also hydration/dehydration cycles. Both framework and extraframework Mn(II) species were suggested to be present.

MnAPSO-44 and MnAPO-44 (CHA topology) were synthesized with cyclohexylamine as a template[66] and characterized by NMR and ESR spectroscopies.[67,68] The ^{31}P, ^{29}Si, and ^{27}Al MAS NMR spectra are similiar to those of the corresponding samples except for significant broadening due to dipolar interaction of part of the framework nuclei with paramagnetic Mn(II). The ESR spectra measured at X- and Q-bands show Mn(II) in the as-synthesized and calcined samples with hyperfine splittings of 85 and 95 G, respectively. While calcination does not change the ESR spectra, dehydration at 400 °C reduced the hyperfine constant to 65 G, indicating a change to tetrahedral coordination upon water removal. Both ^{31}P and ^{27}Al modulation was observed in ESEM measurements. The EPR and ESEM results are interpreted in terms of Mn incorporation into tetrahedral framework sites at least for samples with low manganese content (Mn/P = 0.026). Furthermore, "2 + 1" ESE experiments indicate that only 15% of the Mn(II) ions are homogeneously distributed and contribute to the echo signal in as-synthesized and calcined samples. The amount of homogeneously distributed species in MnAPSO-44 is rather close to that observed in MnAPO-5[58] with similiar Mn content.

MnAPO-31 and MnAPSO-31 have been tested for catalysis of the isomerization of 1-butene, which proceeds by either double-bond or skeletal isomerization. MnAPSO-31 (Mn/P = 0.005) yields the highest percentage of isobutene, whereas AlPO-31 leads almost completely to a double-bond shift whith only minor skeletal isomerization. However, compared to SAPO-31, the increase in selectivity is limited. It is therefore likely that the better catalytic performance corresponds to a higher concentration of acid sites and presumably higher acid strength of these sites.[69]

E. Iron

The question of whether iron can be incorporated into the framework of AlPO-5 was addressed using different techniques such as powder X-ray diffraction, solid-state NMR, ESR, and Mössbauer spectroscopy. The amount of iron reported to be incorporated into FAPO-5 is rather low, therefore changes in the XRD pattern cannot be observed. Typical ESR spectra of as-synthesized FAPO-5 show five distinct signals at $g = 2.0$, $g = 2.2-2.4$, $g = 4.3$, $g = 5.2$, and $g = 8.4$.[70] Signals at $g = 2.0$, $g = 4.3$, and $g = 6.0$ were earlier reported by Park and Chon[71] While the band at $g = 2.0$ has been attributed to octrahedrally coordinated iron in extraframework oxides, the signal at $g = 4.3$ is typically assigned to Fe(III) tetrahedrally coordinated to oxygen.[72,73] Catana et al.[70] suggest that the $g = 2.0$ signal is due to Fe(III) in a tetrahedral site and the $g = 4.3$ line is ascribed to Fe(III) in a distorted tetrahedral (defect) site. The total intensity of these two lines increases linearly with iron concentration, when the saturation level is exceeded.[70] The ESR intensities increase linearly with $1/T$ (Curie−Weiss behavior) in the temperature range of 120−350 K. Similiar results were obtained for FAPO-11 molecular sieve.[74]

Mössbauer spectra of iron substituted AlPO-5 fit a singlet and two doublets showing that there are two types of Fe(III) and one type of Fe(II) present (Figure 7). The singlet (isomer shift $\delta = 0.188$) is assigned to tetrahedral Fe(III) in the framework, while one doublet ($\delta = 0.3$) is assigned to Fe(III) in an amorphous phase.[75] The second doublet ($\delta > 1$) is assigned by Das et al.[75] to divalent iron, which sums to 10−20% in FAPO-5. In FAPO-11 the amount of divalent iron is very low. Cardile et al.[75] also found Fe(II) and Fe(III) in their FAPO-5 samples. Considering that an Fe(III) salt was added to the synthesis gel, some reduction of Fe(III) takes place during sample preparation. If an Fe(II) salt was used as a starting material, a large amount of extraframework iron(II) was found along with Fe(III) in the framework.[77] The Mössbauer spectrum of iron impregnated AlPO-5 exhibits a symmetric doublet due to quadrupolar splitting and an isomer shift near 0.3 mm/s[78] which is attributed to superparamagnetic Fe(III).

Hoppe et al. synthesized FAPO-5 in the presence of methylene blue to obtain innovative materials with special optical properties.[72] Fe(II) ($\delta = 1.4$) was found as well as Fe(II) ($\delta = 0.8$) in the Mössbauer spectra. The addition of methylene blue has no influence on the (Fe(II)/(Fe(III) ratio when $FeSO_4$ is used for the synthesis. The use of Fe(III) leads to irreversible decomposition of the complex.

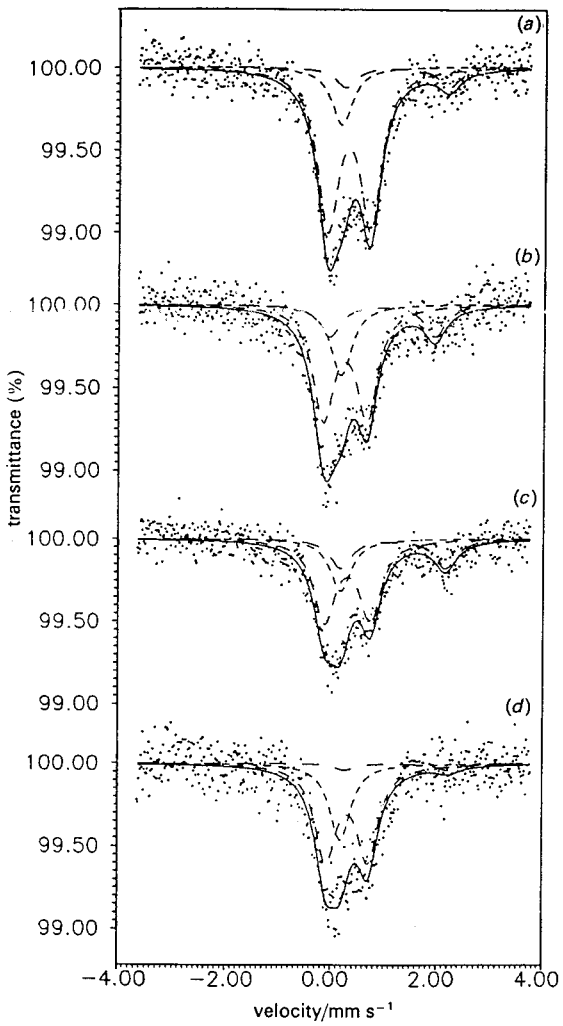

Figure 7. Mössbauer spectra of iron-containing AlPO-*n*: (a−c) FAPO-5 with increasing amount of iron substituted into the framework as determined from ESR spectroscopy and (d) FAPO-11. (Reprinted with permission from ref 75. Copyright 1992 Royal Society of Chemistry.)

Among other methods used for the characterization of FAPO materials photoacoustic spectroscopy gives information on the incorporation of iron into the framework of aluminophosphates.[71] All calcined FAPO-5 samples show spectra with four well-resolved bands at 380, 410, 435, and 480 nm. These bands are also found in as-synthesized Fe silicalite and were assigned to Fe(III) surrounded tetrahedrally by oxygen.[79,80]

Fe/AlPO-5 catalyst prepared by impregnation in aqueous and organic media and subsequently activated by reduction were tested for CO hydrogenation in a stainless steel microreactor at 1.1 MPa and 598 K. It was shown that Fe/AlPO-5 impregnated in aqueous solution shows no activity, while Fe/AlPO-5 impregnated in organic media shows 6 and 23% conversion depending on the type of organic solvent.[78]

Recently, the incorporation of iron(III) into the framework of SAPO-37 (FAU) replacing tetrahedrally coordinated aluminum has been reported by Spinacé et al.[53] Crystallization of FAPSO-37 has been achieved by a slight variation in the gel composition and synthesis temperature compared to that for SAPO-37. The UV−vis diffuse reflectance spectrum of

FAPSO-37 shows two bands at $\lambda = 215$ and 250 nm, which are assigned to charge transfer from oxygen to an isolated framework Fe(III). Also a very weak band at 370 nm is observed, which is assigned to forbidden d−d transitions of iron(III) in tetrahedral coordination confirming the incorporation of iron into the lattice. Two ESR signals at $g = 4.3$ and $g = 2.0$ were observed and assigned to framework-incorporated Fe(III) and hydrated Fe(III).

^{57}Fe Mössbauer spectroscopic studies were carried out on ferrocene guest molecules in AlPO-5 and AlPO-8 at 300 and 20 K.[81] The room-temperature spectrum shows complete orientational freedom including flipping between parallel and perpendicular orientations which is still rapid on the Mössbauer time scale, whereas the low-temperature spectrum shows either fixed molecules or rotations which are slow on the Mössbauer time scale.

F. Cobalt

The synthesis of cobalt-containing aluminophosphates has been described in many papers,[82−87] and the preparation of large CoAPO-5 crystals has been achieved.[88,89] The isomorphous substitution of cobalt into AlPO-*n* and SAPO-*n* has been studied extensively with many different techniques and in numerous structures including -5, -11, -14, -18, -25, -34, -36, -41, -44, and -50.[90−97] In some of these structures cobalt can only be incorporated into SAPO materials.[98] ESR studies in cobalt-containing aluminophosphates are relatively rare, since the electron-spin relaxation is so rapid as to require temperatures below 30 K to allow observation of Co(II). Initial studies by Iton et al.[100] in CoAPO-5, CoAPO-34, and CoAPSO-34 at 4.2 K showed ESR of Co(II) with $g = 5-6$. Calcination of as-synthesized materials led to a significantly reduced intensity of the Co(II) ESR signal intensity. This reduced intensity (∼23%) was ascribed to oxidation of Co(II) to Co(III) during the calcination procedure.

A sharp signal ($g = 2.03$) was reported at room temperature by Montes et al.[92] in as-synthesized CoAPO-5, which was ascribed to Co(II) being in a framework position. After ion-exchange of the sample with 0.1 N NH_4Cl and calcination, this sharp signal was not observed, but a very broad signal was seen at 77 K. This was explained by the authors as evidence for the oxidation of Co(II) to Co(III), but this interpretation is unclear. A similar signal ($g = 2.05$) was found by Prakash et al.[99] in their studies of CoAPO-5 using a different template for the synthesis. However, quantitative comparison of the experimental data on the amount of Co(II) in as-synthesized, calcined, and calcined followed by hydrogen- or methanol-treated CoAPO-5 samples indicate some disagreement between the results of different groups.[100−102]

Temperature-programmed desorption (TPD) and thermogravimetric analysis (TGA) of amine probe molecules show that Co(II) at low concentrations is present in lattice positions and generates discrete Brønsted sites in a concentration equal to the cobalt content in *both* as-synthesized blue CoAPO-5 and calcined yellow-green CoAPO-5 consistent with no oxidation associated with the color change.[101] On the basis of this finding, Kurshev et al.[102,103] performed ESR experiments from 7 to 34 K. The experimental data in this temperature range show that the ESR signal of Co(II) in calcined CoAPO-5 does not follow the Curie law and therefore that the ESR intensity of calcined samples is *not* directly associated with the amount of paramagnetic cobalt. The intensity of the doubly integrated spectra as a function of the temperature of as-synthesized and calcined CoAPO-5 is displayed in Figure 8. At temperatures higher than 20 K no differences can be seen, which shows that the amount of Co(II) does not change upon calcination. The temperature dependence of the ESR intensity follows the Curie law in as-synthesized CoAPO-5, but calcined CoAPO-5 exhibits an abnormal temperature behavior, which is well explained by a distortion of the tetrahedral symmetry of Co(II) to a lower dihedral symmetry by interaction of two oxygen molecules with cobalt. The anomalous temperature dependence of the ESR intensity of Co(II) in calcined CoAPO-5 can then be quantitatively explained by a negative zero-field splitting between the $M_s = \pm 1/2$ and $M_s = \pm 3/2$ Kramers doublets. When the temperature decreases, the Cu(II) ions tend to populate the $M_s = \pm 3/2$ level, which is not ESR active, and the intensity of the observed ESR transition between $M_s = +1/2$ and $M_s = -1/2$ decreases. Therefore, changes of the local symmetry near the cobalt ion seem responsible for the intensity loss of the ESR signal rather than a change in the oxidation state. These conclusions were also supported in two other independent studies[104,105] using IR and UV−vis spectroscopy.

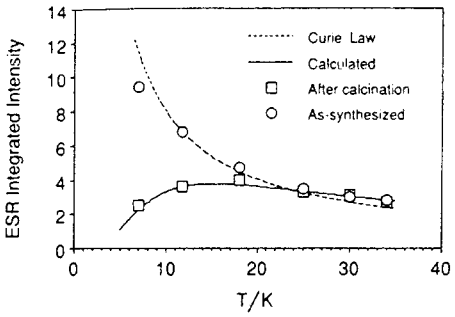

Figure 8. Doubly integrated ESR spectral intensity of Co(II) ions in as-synthesized and calcined CoAPO-5 from 7 to 34 K. The solid curve represents the calculated ESR absorption. (Reprinted with permission from ref 102. Copyright 1994 American Chemical Society.)

The use of NMR spectroscopy in characterizing cobalt-containing AlPOs has gained some credence recently following the work of Canesson et al.[106] and Van Breukelen et al.[107] The presence of cobalt in AlPOs typically results in signal boadening or the appearance of multiple peaks. Usually, ^{31}P and ^{27}Al MAS NMR studies on CoAPOs and CoAPSOs cannot be used in the same way as suggested for magnesium-containing MAPO-20,[108,109] although this concept has invoked some criticism recently.[110,111] Montes et al.[93] observed that compared with AlPO-5, the NMR spectrum of CoAPO-5 contained multiple and intense sidebands which indicates increased anisotropy. They ascribed this increase in anisotropy to strong dipolar

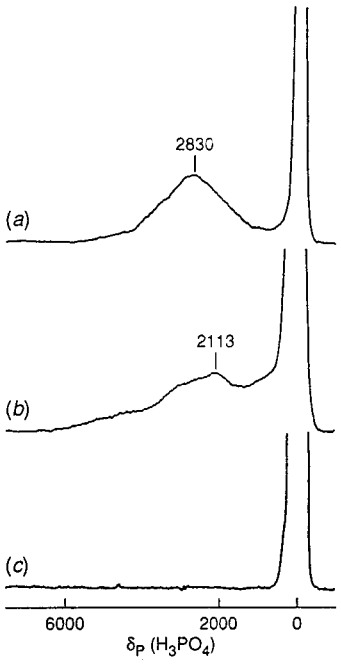

Figure 9. ^{31}P NMR spectra by spin−echo mapping of (a) as-synthesized CoAPO-5, (b) calcined CoAPO-5, and (c) cobalt impregnated Co/$AlPO_4$-5. (Reprinted with permission from ref 106. Copyright 1997 Royal Society of Chemistry.)

coupling of phosphorus with paramagnetic Co(II) and, hence, as evidence for framework incorporation of Co(II) replacing aluminum. The observation of intense sidebands is reported by several authors,[99,112,113] while in other studies no such increase indicating increased anisotropy was reported.[107,114] However, measurements of impregnated Co/AlPO-5 and Co/AlPO-11[112,55] also showed NMR sidebands consistent with increased anisotropy. Therefore, such increased anisotropy cannot be used as evidence for isomorphous substitution of cobalt into aluminophosphates.

Prakash et al.[113] suggest that the broad peak for CoAPSO-46 is caused by the presence of two signals, namely P_1(3 Al, 1 Co) and P_2(4Al). Recent results suggest that the P_1(3 Al, 1 Co) is broadened and/or displaced beyond detection under the conditions of routine NMR measurements. Due to dipolar interaction of phosphorus with the nearby paramagnetic cobalt, these signals are moved over large distances and cannot be excited when the irradiation frequency is centered at $\delta = 0$ ppm. Canesson and Tuel showed for CoAPOs that a signal for P_1(3 Al, 1 Co) is found at about $\delta = 2500$ ppm (Figure 9).[106] They suggest that for every cobalt which is a direct neighbor to phosphorus, about 2500 ppm should be added to find a NMR signal for the phosphorus near cobalt. Application of the usual inversion−recovery sequence distinguishes the relaxation processes of ^{31}P nuclei between CoAPO-*n* and impregnated Co/AlPO-*n* molecular sieves.[115] The values of decay time for zero intensity for ^{31}P NMR signals in an inversion−recovery sequence are much reduced in CoAPO-5 in comparison to Co/AlPO-5.

The clustering of cobalt in CoAPO-5 has been studied by Van Breukelen et al.[107] employing quantitative ^{31}P NMR spectroscopy. They found that with increasing cobalt-content in CoAPO-5 from 0.001 to 3.15 wt. % the percentage of NMR-visible cobalt decreases from 97 to 42%. If the existence of extraframework cobalt can be ruled out, then around 10 NMR-invisble phosphorus atoms per cobalt atom are needed to explain the observed decrease in signal intensity. The amount of NMR-invisible phosphorus cannot be explained by assuming that only ^{31}P signals of phosphorus in the first coordination sphere (four) become invisible. In contrast, if one assumes that the phosphorus atoms in the first and the third coordination sphere become invisible, then the amount of NMR-invisible phosphorus per cobalt becomes 25, which is too high. A possible explanation for these observations is the formation of cobalt clusters of five or more cobalt atoms, which leads to about 10 NMR-invisible phosphorus per cobalt atom.

While the isomorphous substitution of cobalt into several AlPO-*n* structures is commonly accepted, there is controversy about the redox properties of cobalt-containing AlPOs involving Co(II) and Co(III) valence changes which is of considerable importance for redox reactions. The blue color of as-synthesized materials is considered characteristic of tetrahedral $Co^{II}O_4$ environments and is therefore consistent with cobalt occupying tetrahedral framework sites. Tetrahedral coordination of cobalt is also attributed to d−d electronic transitions in UV−vis spectra. Calcining blue materials at 400 to 500 °C causes the color to change to green, green-yellow, or beige for high, medium, and low cobalt contents, respectively. It was suggested that these color changes reflect varying degrees of oxdiation to cobalt(III),[100,113,116−118] which might be dependent on the structure type.[119] Barrett et al. have used X-ray absorption spectroscopy to investigate different cobalt-containing materials after synthesis, calcination, and reduction.[118] They found that while in as-synthesized materials Co(II) is in a regular four-coordinated site, the situation is more complex in calcined materials. In CoAPO-18 essentially complete oxidation of Co(II) to Co(III) is deduced with the local coordination of high-spin Co(III) being distorted. In contrast, incomplete oxidation was deduced for CoAPO-5 and CoAPO-36. Chao et al.[120] investigated the redox behavior in CoAPO-5 using ESR and IR spectroscopy. They explained the behavior of cobalt in terms of a species that they characterized as a dioxygen complex O_2−CoAPSO-5 in which the framework tetrahedral $Co^{II}O_4$ increases its coordination and valence state by attaching a O_2^+ molecular ion to form the complex. Recently, Wu et al.[121] proposed a dioxygen−cobalt species in CoAPO-11 on the basis of their combined analysis of Raman and ESR spectroscopies. Calcination at 550 °C yields a diamagnetic hydroperoxo Co−O−O−H species, which shows a Raman band at 1019 cm^{-1}. After subsequent hydrogen reduction followed by O_2 adsorpion, a superoxo-like cobalt species (Co−O−O$^\bullet$) is generated (Figure 10b) with an assigned ν(O−O) Raman band at 1048 cm^{-1}. The O−O and Co−O stretching modes were further confirmed by $^{16}O_2/^{18}O_2$ isotope substitution.

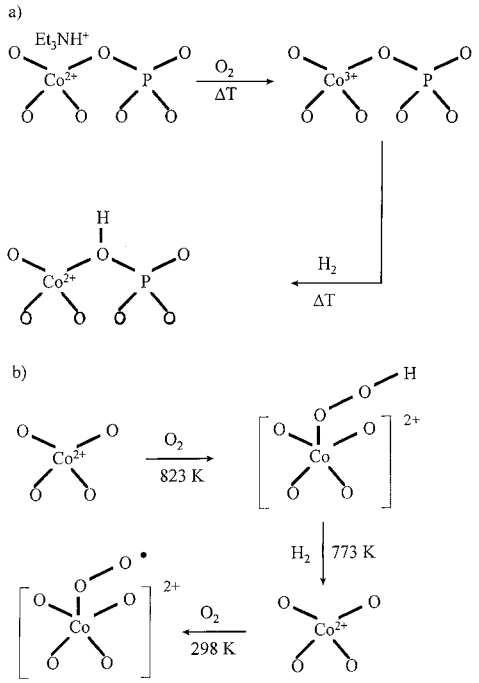

Figure 10. Proposed model for cobalt species in CoAPO-*n* under redox treatment according to (a) Verberckmoes et al.[124] and (b) Wu et al.[121]

Diffuse reflectance UV−vis spectroscopy has been frequently employed for the characeterization of cobalt-containing aluminophosphates.[112,123,124] As-synthesized CoAPO-5 has been characterized by a triplet at 16 000, 17 300, and 18 500 cm^{-1}, which corresponds to 625, 578, and 541 nm.[112,116,122,123,125,126] These absorptions are interpreted as due to Co(II) in a tetrahedral environment of oxygens in the AlPO framework. After calcination the intensities of these bands are reduced and the band positions shift to 15 500 cm^{-1} (645 nm), 17 300 cm^{-1} (578 nm), and 19 500 cm^{-1} (513 nm). New intense bands also arise around 25 200 cm^{-1} (400 nm) and 31 500 cm^{-1} (317 nm). This spectrum is ascribed to Co(II) in a tetrahedrally distorted environment and to Co(III). This structural Co(III) is then reported to be reducible with hydrogen, carbon monoxide, NO, methanol, acetone, toluene, and water.[105] Spectroscopic criteria for the distinction between framework and extraframework Co(II) in CoAPO-5 were recently presented by Verberckmoes et al.[124] Tetrahedral Co(II) in the lattice after calcination is assigned to bands at 5500 and 15 150 cm^{-1}. Tetrahedral Co(II) in extraframework positions is assigned to bands at 5500 and 16 850 cm^{-1}, while octahedral Co(II) in extraframework positions is assigned to bands at 8100 and 19 550 cm^{-1}. Upon calcination (pseudo) tetrahedral Co(III) in the framework, (pseudo) octahedral Co(II) in extraframework sites and (pseudo) tetrahedral Co(II) in both framework and extraframework sites are formed depending on the crystalline quality of the sample. Upon subseqent reduction Co(III) is transformed to tetrahedral Co(II) in the lattice with formation of an OH bond with a typical streching frequency of 3530 cm^{-1} (Figure 10a).

However, the mechanism of the redox process is still under discussion, and there is disagreement as to the existence of trivalent cobalt in the calcined materials. Instead, it has been suggested that the color changes are the result of distortions of the symmetry of the original tetrahedral environment. The redox properties of CoAPO-5 and CoAPO-44 have been investigated by Berndt et al.[105] by temperature-programmed reduction, oxidation, and desorption. Furthermore, the acidity of the samples after oxidation or reduction treatments was investigated by temperature-programmed desorption of ammonia and FTIR using pyridine as a probe molecule. Berndt et al.[105] found no evidence for a valence state change of a significant portion of the framework cobalt ions or of adsorption of oxygen on such sites. The formation of framework Co(III) from Co(II) was also not supported by Lohse et al.[110] who conducted IR investigations of basic probe molecules (NH_3, pyridine, and acetonitrile) adsorbed on CoAPO-5 and CoAPO-44. The insertion of one Co(II) ion into an aluminum or a phosphorus site creates one acid site. To describe the acid site, Marchese et al.[127] proposed an equilibium between bridging hydroxy groups, paired centers of Lewis sites and POH groups as in the reaction shown in eq 2. It is of note that the presence of Lewis acid sites, such as the unsaturated cobalt presented in structure B in eq 2 is revealed by adsorbing water,[127] ammonia,[104] acetonitrile,[108] or carbon monoxide.[104,129]

$$\underset{\text{A}}{\text{P(OH)}-\text{Co}^{\text{II}}\text{O}} \leftarrow \underset{\text{B}}{\text{P(OH)}\cdots\text{Co}^{\text{II}}\text{O}_3} \qquad (2)$$

The correlation between cobalt framework substitution and acidity has been investigated in a series of papers by Thomas and co-workers[127−130] mainly aiming at solid acid catalysts for methanol conversion to light olefins. To overcome the difficulties in revealing the Bronsted acidity of CoAPO catalysts, Thomas and co-workers proposed the use of nitrogen as a molecular probe, which is considered to be advantageous because nitrogen is a weaker base and is unlikely to affect the catalytic centers.[131] The bridged OH streching mode is shifted 100 cm^{-1} to lower energy by adsorbing N_2 at 77 K because of the formation of a weak H-bond. This shift is about 10−20 cm^{-1} smaller than that of the OH in H−ZSM-5, which suggests a lower Bronsted acidity for CoAPO-18 compared to H−ZSM-5. The downward shift of the stretching and the upward shift ($\Delta\delta_{OH} = +14$ cm^{-1}) of the bending frequencies of the P−OH groups upon adsorption of nitrogen is evidence for the formation of H-bond complexes between N_2 and OH.[131] The adsorption of more basic probe molecules can greatly affect the strength of the Co−O bond in structure B in eq 2.

The local environments of cobalt atoms in as-synthesized, calcined, and hydrogen-reduced CoAPSO-34 have been studied by X-ray absorption spectroscopy.[132] Cobalt is shown to be sited as Co(II) in the framework and calcination of CoAPSO-34 (4.4 wt % Co) leads to two-thirds of the Co(II) being oxidized to Co(III). Reduction of the sample leads to materials containing only Co(II). The XANES spectra and their derivatives (Figure 11) show a single edge peak at 7718 eV for as-synthesized CoAPSO-34 which is

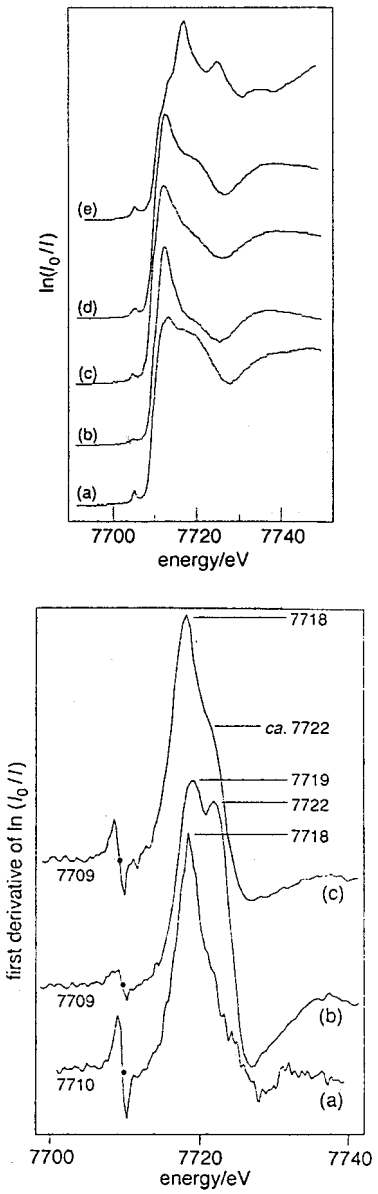

Figure 11. Normalized Co K-edge Xanes (left side) and first derivative (right side) of the Xanes region of (a) as-synthesized CoASPO-34, (b) calcined CoAPSO-34, (c) subsequently reduced CoAPSO-34, (d) reference compound DAF-2, and (e) reference compound $CoAl_2O_4$. (Reprinted with permission from reference 132. Copyright 1997 Royal Society of Chemistry.)

assigned to Co(II). After calcination an additional peak at 7722 eV appears which is assigned to Co(III). After subsequent reduction the 7722 eV peak only partially disappears. The change of the local environment of Co in CoAPO-18 has been investigated by combined use of EXAFS and XANES.[130] The oxidation of Co(II) to Co(III) during calcination results in a displacement of the K-edge by 1.2 eV, an increase of the structure before the edge at 7710 eV and a reduction of the frequency of the EXAFS vibrations. This reduction reflects a decrease in the Co−O bond length from 0.195 nm in as-synthesized CoAPSO-34 to 0.183 nm in calcined CoAPSO-34. Upon reduction, the bond length increases to 0.19 nm. Detailed EXAFS investigations showed that tetrahedral Co coordination is slightly disordered, which is due to one Co−O bond being substantially

Figure 12. ESR spectrum at 77 K of isolated Ni(I) in NiH-SAPO-11.

longer (0.204 nm). A possible explanation is the protonation of the respective oxygen.[130]

Photoacoustic spectroscopy was applied to obtain depth-resolved information on CoAPO-44.[133] The spectra showed the presence of tetrahedral framework cobalt ions and cobalt with lower symmetry. The lower symmetry cobalt is more concentrated in the inner part of the crystallite of as-synthesized CoAPO-44, while it is distributed rather uniformly in the calcined sample. The spectra of CoAPO-5 and CoAPO-11 have shown in agreement with results by Schoonheydt et al.[116] that the amount of cobalt that can be incorporated is limited to about 0.5 mol %.[134] ESR spectra revealed that allyl- or cation-type radicals were formed via interaction with framework cobalt ions upon adsorption of alkenes such as cyclohexene, cyclopentene, and tetramethylethene.

G. Nickel

Ni(I) in Ion-Exchange Sites

Because of their catalytic importance, nickel species have been studied intensively in SAPO materials.[135] Ni(II) can be readily exchanged into silicoaluminophosphates utilizing a solid-state ion-exchange reaction between the molecular sieve and a nickel salt. It is of particular interest that the paramagnetic valence state nickel(I) can be stabilized in these materials.[136−140] γ-Irradiation at 77 K can be used to generate nickel(I), but this method is often inefficient and is therefore not used very much.[141] A better way to reduce nickel(II) is by hydrogen reduction at 473−573 K under 100−500 Torr of hydrogen. Hydrogen reduction is complicated by the formation of metallic nickel in addition to nickel(I), so that particular care is needed to establish the conditions of temperature, hydrogen pressure, and reduction time for generation of a suitable concentration of nickel(I) species.[136,138−143] A third possibility is to utilize thermal autoreduction which takes place when a hydrated molecular sieve is dehydrated under vacuum at temperatures above 573 K. Particular care is needed to avoid formation of superferromagnetic nickel(0) ($g = 2.25$) which is thermodynamically more stable than Ni(I).[141,144]

ESR studies of nickel(I) in SAPOs must be carried out carefully since Ni(I) is readily oxidized by water or oxygen. Figure 12 shows the signal of an isolated Ni(I) species which is axially symmetric ($g_{||} = 2.49$, $g_{\perp} = 2.11$). This species can be generated by thermal or hydrogen reduction. The location of the active species is of great importance for catalytic applications. The location of nickel(I) has been determined at various stages of dehydration.[139,140] But the ESR spectra alone do not reveal such information, since the changing g values are not discriminatory. A

Table 5. ^{31}P ESEM Parameters for Ni(I) in NiH-SAPO-11 and NiH-SAPO-5

sample	dehydration temp	shell	N	R/ nm	A_{iso}/ MHz	site
NiH-SAPO-11	473	1	3.6	0.33	0.59	near SII
		2	7.2	0.60	0.18	
	773	1	5.3	0.34	0.50	SI
		2	12.3	0.70	0.12	
NiH-SAPO-5	573	1	3.5	0.28	0.42	near SII
		2	4.5	0.60	0.10	
	773	1	5.2	0.33	0.56	SI
		2	10.5	0.72	0.01	

powerful tool is ^{31}P ESEM spectroscopy, where a significant difference in the spectra recorded after dehydration at 473 and 773 K can be detected. The simulation parameters for the ^{31}P modulation for these two conditions are listed in Table 5.[139,140] It is deduced that Ni(I) is located in the center of a hexagonal prism (site SI) since $N = 5.3$ after dehydration at 773 K. The same nickel locations are observed after hydrogen reduction of NiH-SAPO-5 and NiH-SAPO-11. At lower dehydration temperatures nickel(I) is located near SII sites since $N = 3.6$.

After exposure to polar adsorbates such as water, methanol, or ammonia the g values of the ESR spectra change in less than 5 min.[140] However, for less polar adsorbates such as ethylene the development of the new g parameters takes a longer time and even a higher temperature (353 K) in the case of NiH-SAPO-11. It has been concluded that Ni(I) has to migrate from site I to a site in a large channel, most likely site SII*, to interact with the adsorbate molecules.

Ni(II) introduced by ion-exchange into SAPO-41, which is a medium pore molecular sieve with a novel structure involving adjacent 10-ring channels, forms Ni(I) by thermal reduction. Ni(I) in SAPO-41 decomposes water but forms complexes with ammonia, methanol, and ethylene.[145] The location of Ni(I) in a main 10-ring channel near a 6-ring window was determined by ^{31}P ESEM.

Ni(I) in Framework Sites

The interesting question of whether Ni(I) can be incorporated into an aluminophosphate or silicoaluminophosphate framework has prompted several studies in different structure types. Among these are NiAPO-5 and NiAPSO-5,[142,143,146−148] NiAPO-11 and NiAPSO-11,[139,143,149] NiAPSO-34 and NiAPSO-34,[150−152] and NiAPO-20[153] and NiAPSO-41.[154] The synthesis is usually attempted by adding a nickel salt ($NiCl_2 \cdot 6H_2O$ or $Ni(CH_3COO)_2$) to the synthesis gel. But actual framework incorporation is difficult to prove. After the synthesis and subsequent thoroughly washing, nickel can be found by chemical analysis in the crystalline product. An observed increase of acidity gives only limited evidence for nickel being in a framework site.[2] All investigations show that the amount of nickel, if any, which can be incorporated into the framework is relatively low.

ESR and ESEM spectroscopy are useful tools for evaluation of the possible incorporation of nickel into the SAPO framework.[138,142,143] A recent study on nickel in AlPO-5 and AlPO-11 reveals a room-temperature ESR spectrum, which exhibits two transitions with parameters $g_{\|} = 2.09$ and $g_{\perp} = 2.07$ for NiAPO-5 and $g_{\|} = 2.08$ and $g_{\perp} = 2.07$ for NiAPO-11. These ESR spectra were recorded directly after calcination and ascribed to nickel in framework positions.[149]

Table 6. ^{31}P ESEM Data of Nickel(I) in Ion Exchange versus Framework Positions

sample	shell	N	R/nm
NiAPSO-5	1	8.8	0.51
	2	24.5	0.97
NiAPSO-11	1	10.5	0;.52
	2	30.1	0.95
NiAPSO-41	1	12	0.54
	2	10	0.78
theory: P-site	1	10−12	0.5−0.6
	2	28	0.9−1.0
NiH-SAPO-5	1	5.2	0.33
	2	10.5	0.72
NiH-SAPO-11	1	5.3	0.34
	2	12.3	0.70
NiH-SAPO-41	1	2	0.35
	2	3	0.59
theory: SI position	2	10−12	0.65−0.75

A better approach to ESR spectroscopic detection is the reduction of nickel(II) to nickel(I) by thermal or hydrogen reduction and subsequent ESR and ESEM measurements at 77 and 4 K, respectively. While the ESR spectra of Ni(I) in ion-exchanged or synthesized Ni materials are not very different, ^{2}D and ^{31}P ESEM data provide clear evidence for framework incorporation of Ni(I). There is a significant difference in the ^{31}P modulation pattern between Ni(I) in ion-exchange sites and Ni(I) in framework positions (Table 6). It has been deduced that Ni(I) ions in NiH-SAPO-5 and NiH-SAPO-11 are located in the center of a hexagonal prism site (SI) since the number of nearest phosphorus atoms (N) is 5.2 and 5.3, respectively (Table 6). After hydrogen reduction Ni(I) occupies the same positions as after dehydration at temperatures above 773 K.

The ESEM data for Ni(I) in NiAPSO-5, NiAPSO-11, and NiAPSO-41 are consistent with nickel replacing phosphorus in the original alternating Al−O−P framework.[142,143,154] The simulation data (Table 6) show 8.8, 10.5, and 12 nearest P atoms at a distance of 0.5 nm. If nickel is in an aluminum site the experimental data should show four nearest P at a distance of about 0.31 nm.

From methanol adsorption other evidence for a location difference of Ni(I) between NiAPSO-5 and NiH-SAPO-5 can be obtained. In NiH-SAPO-5 a species with $g_{\|} = 2.574$ and $g_{\perp} = 2.063$ is seen after methanol adsorption. In contrast, NiAPSO-5 shows a sharp signal with $g_{\|} = 2.385$ and $g_{\perp} = 2.132$. Since these g values obviously differ from those of isolated Ni(I), methanol coordination is indicated and supported by the ESEM data (Table 7). From these data distinctly different coordination geometries with methanol and ethylene are derived as shown in Figures 13 and 14. A possible explanation is as follows.

In the case that nickel substitutes for phosphorus in the framework, Ni(I) can be regarded as a locally negative site. The adsorbate coordination geometry

Table 7. ESEM Parameters for Ni(I) with Adsorbed Methanol in Different SAPO Materials

sample	shell	*N*	*R*/nm	A_{iso}/MHz
NiH-SAPO-5				
CH_3OD	1	2	0.29	0.43
	2	1	0.31	0.10
CD_3OH	1	6	0.34	0.21
	2	3	0.40	0
NiAPSO-5				
CH_3OD	1	2	0.25	0.15
	2	1	0.35	0
CD_3OH	1	6	0.33	0.08
	2	3	0.36	0.0
NiH-SAPO-11				
CH_3OD	1	1	0.28	0.43
CD_3OH	1	3	0.36	0.26
NiAPSO-11				
CH_3OD	1	1	0.24	0
CD_3OH	1	3	0.32	0.16

of methanol in NiAPSO-5 and NiAPSO-11 is consistent with this. In NiAPSO-11 Ni(I) interacts with one methanol molecule in an orientation geometry typical for the coordination of small polar molecules to anions.[12] A similar OD bond orientation is found in NiAPSO-5 (Figure 13), but due to the bigger channel size two methanol molecules are so coordinated. The methanol coordination in NiH-SAPO-5 and NiH-SAPO-11 is different and typical for exposed cations in ion-exchange sites. The methanol is oriented with the partially negatively charged oxygen toward the nickel ion. In NiH-SAPO-5 due to the increased channel size Ni(I) is coordinated to three methanol molecules compared to one methanol molecule in NiH-SAPO-11. These results show substantial differences between synthesized and ion-exchanged materials. Similar results have been found in previous work for manganese ion incorporation into SAPO-11.

ESEM analysis of adsorbed ethylene also shows evidence for a difference between Ni(I) in ion-exchanged and framework sites of nickel(I) species showing almost identical ESR spectra. For the ion exchanged samples the π-bond of one ethylene is coordinated with its molecular plane perpendicular to a line toward the nickel atom (Figure 14). This is a typical geometry that has been found for ethylene coordination to a variety of transition metal ions in ion-exchange sites of molecular sieves. The ESEM data for NiAPSO-5 and NiAPSO-11 show a different coordination geometry for C_2D_4 with nickel(I) indicating that π-bonding is not present (Table 8). The distances to the more distant D nuclei are in agreement with the known ethylene structure assuming weak σ-bonding. Since this type of bonding is only present in NiAPSO-5 and NiAPSO-11, it can be assumed that π-bonding is inhibited due to steric hindrance which is evidence for Ni(I) being in a framework site. The increasing number of adsorbates reflects the change in channel size. The different ESR spectra and the ESEM results show that the local environment of Ni(I) in synthesized NiAPSO-*n* is different from that of ion-exchanged NiH-SAPO-*n*. Therefore the results support that Ni(I) occupies a framework position in NiAPSO-11 and NiAPSO-5 with unique adsorbate coordination geometries.

H. Palladium

Paramagnetic palladium species have been studied by ESR and ESEM spectroscopy in SAPO-5 and SAPO-11[156−160] and in SAPO-34.[161] It has been found that in contrast to zeolite X and Y, SAPO materials are not able to stabilize paramagnetic Pd(III) species; therefore only paramagnetic Pd(I) is found. To prepare palladium(I) in silicoaluminophosphates, the tetrammine complex of Pd(II) is well mixed with the molecular sieve powder which is then heated in a vacuum to about 450 °C. Subsequently, a complex activation method (dehydration at 450 °C, oxidation at 500 °C, evacuation at 500 °C) leads to the formation of Pd(I) as detected by ESR. After dehydration at 450 °C no Pd(I) can be detected which is most likely due to autoreduction of Pd(II) to form small Pd(0) clusters (eq 3).

$$\mathrm{Pd(II)} \xrightarrow{\text{dehydration}} \mathrm{Pd(0)\ clusters} \qquad (3)$$

$$\mathrm{Pd(0)} \xrightarrow[823\ \mathrm{K}]{\text{oxidation}} \mathrm{Pd(II)} \qquad (4)$$

$$\mathrm{Pd(0) + Pd(II)} \xrightarrow[823\ \mathrm{K}]{\text{evacuation}} \mathrm{2Pd(I)} \qquad (5)$$

Oxidation of these Pd clusters is possible to form Pd(II) (eq 4) although this oxidation might not be quantitative. Again after this treatment no ESR signal is detected. In the final activation step the sample is evacuated at high temperature. The formation of Pd(I) during this treatment is not fully understood but may involve the disproportionation reaction shown in eq 5.[162]

Regardless of the mechanism of the formation of the Pd(I) species, the main question concerns the location of these species. As seen from the ESR spectrum (Figure 15) two different Pd(I) species A and B are formed. The different locations can be determined from ^{31}P modulation.[160] Simulation of the nuclear modulation in terms of the geometry of nearby phosphorus nuclei identifies Pd(I) species A as located in a hexagonal prism site (site I) and Pd(I) species B as located at site II* near a 6-ring window. A change of this location is observed if different adsorbates are introduced into the system. Signal A usually disappears after adsorption of methanol, which indicates a migration of Pd(I) from inaccessible site I to a site close to a main channel (site II or II*).

ESR and ESEM spectroscopic methods have been used to deduce several adsorbate geometries of Pd(I) in PdH-SAPO-11 and PdH-SAPO-5 molecular sieves. The adsorption of water, ammonia, carbon monoxide, hydrazine, and benzene was investigated. The ESR parameters are very sensitive to the interaction of Pd(I) with different adsorbates. Pd(I) is coordinated to two molecules of ammonia and CO, which is derived from the ^{14}N and ^{13}C superhyperfine splitting lines, respectively. Only one molecule of benzene and of pyridine is coordinated to the paramagnetic center. Analysis of the three pulse ESEM spectra of PdH-SAPO-11 indicates interaction with

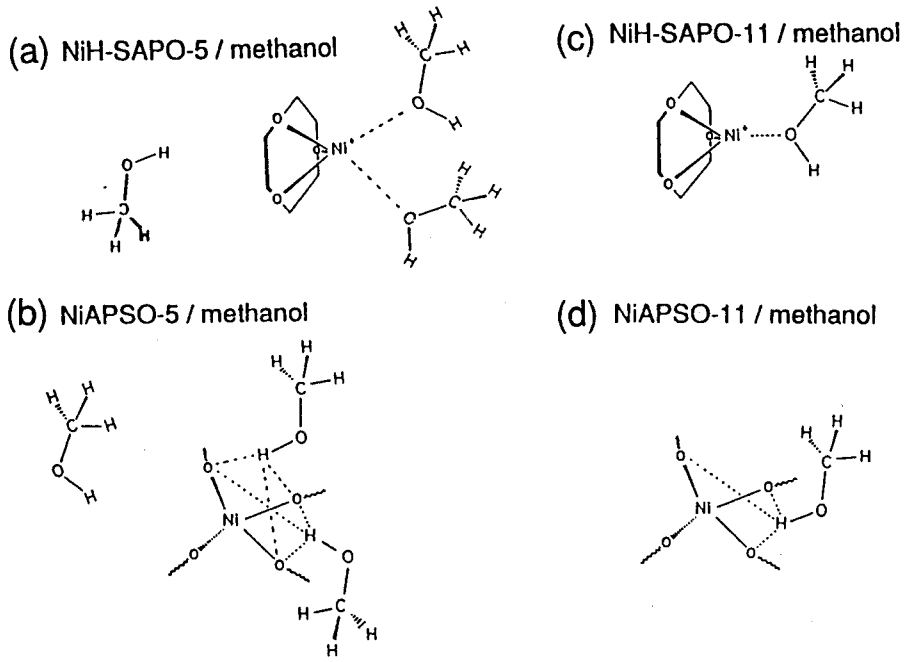

Figure 13. Schematic diagram of Ni(I) coordinated to methanol in (a) NiH-SAPO-5, (b) NiAPSO-5, (c) NiH-SAPO-11, and (d) NiAPSO-11. (Reprinted with permission from ref 143. Copyright 1995 Elsevier.)

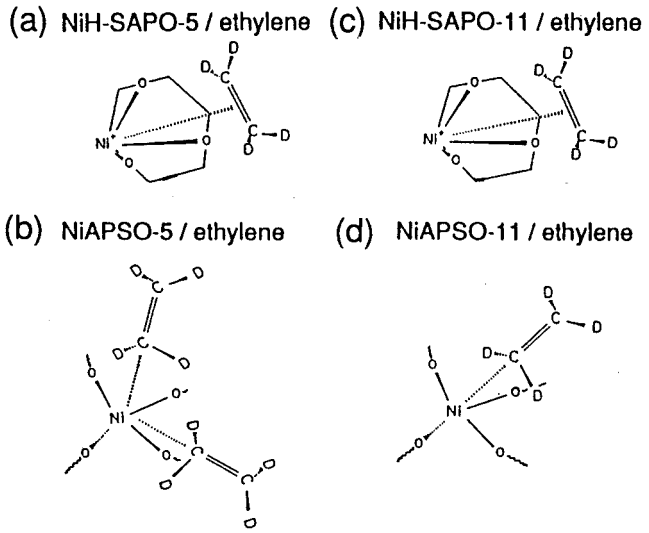

Figure 14. Schematic diagram of Ni(I) coordinated to ethylene in (a) NiH-SAPO-5, (b) NiAPSO-5, (c) NiH-SAPO-11, and (d) NiAPSO-11. (Reprinted with permission from ref 143. Copyright 1995 Elsevier.)

Table 8. Three-Pulse ESEM Simulation Parameters for Deuterium Modulation of Ni(I) with Adsorbed Ethylene

sample	shell	*N*	*R*/nm
NiH-SAPO-11	1	4	0.34
NiH-SAPO-5	1	4	0.35
NiAPSO-11	1	2	0.27
	2	2	0.47
NiAPSO-5	1	4	0.31
	2	4	0.55

four deuteriums (two water molecules) at a distance of 0.35 nm. In both structure types the Pd−H_2O complex is suggested to be located at SII* sites.[157,159]

The introduction of Pd into the framework of SAPO-5 and SAPO-11 was also attempted. ESR and ESEM results reveal no significant differences between ion-exchanged and synthesized palladium containing SAPO-11. It was found that in the range 0.5−1.0 mol % Pd in PdSAPO-11, it is most probable that the palladium ions are not incorporated into framework sites.[156]

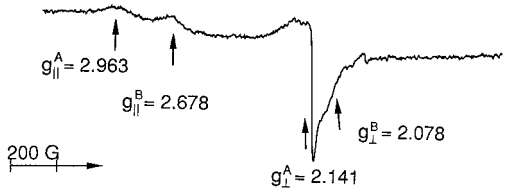

Figure 15. ESR spectrum at 77 K of Pd(I) in PdH-SAPO-11. (Reprinted with permission from ref 220. Copyright 1996 American Chemical Society.)

Electron spin resonance investigations of Pd(I) introduced into SAPO-34 via a solid-state reaction show three different Pd(I) species with different $g_{\perp}$, but with a common $g_{\parallel} = 2.92$. These were ascribed by Back et al.[161] to three different cation site locations. On the basis of adsorption experiments and ^{31}P ESEM analysis, species A_1 ($g_{\perp} = 2.177$) is assigned to the least accessible site I in the center of a hexagonal prism, A_3 ($g_{\perp} = 2.070$) to site II* displaced from a 6-ring into an ellipsoidal cage and A_2 ($g_{\perp} = 2.136$) to the most accessible site IV near an 8-ring window. Adsorption of alcohols such as methanol and ethanol causes a change in the ESR spectrum, which indicates some relocation of Pd(I) to allow better coordination with alcohol molecules. In contrast to PdH-SAPO-5 and PdH-SAPO-11, it was found on the basis of resolved superhyperfine splittings that three molecules of CO and only one molecule of NH_3 coordinate to Pd(I), respectively.

Palladium ion-exchanged SAPO-5 has been used as a catalyst for low-temperature combustion of methane.[163] A high dispersion of Pd was attained and

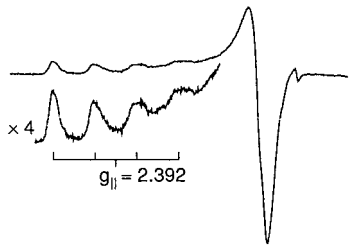

Figure 16. ESR spectrum of Cu(II) in CuH-SAPO-34.

a CH_4 conversion of 90% was achieved at 753 K, which is 200 K lower than for a conventional Pd/Al_2O_3 catalyst.

The isomerization of *n*-heptane was reported over a series of bifunctional SAPO-based catalysts, which contain 0.1 wt % palladium.[164] The best activities and selectivities for branched heptane isomers are achieved with SAPO-11 and SAPO-31; SAPO-17 and SAPO-5 show substantially lower activities. With SAPO-5, there is high cracking activity, which is assumed to be caused by reduced accessibility of bridged hydroxyl groups within the molecular sieve framework. Different locations of these acid sites are evidenced by IR spectroscopy recorded after adsorption of *n*-heptane.[164]

I. Copper

Cupric Ions in SAPO-5 and SAPO-11

Cupric ions have proved to be very fruitful probes in molecular sieves. Of particular interest is the fact that the cupric ion relocates upon partial or complete dehydration of a silicoaluminophosphate. Also the presence of different adsorbates affects the location and coordination of the Cu^{2+} cation in silicoaluminophosphates.[6,165−169]

Figure 16 shows a typical cupric ion ESR spectrum. It is characterized by significant axial *g* factor anisotropy with $g_{||}$ at lower magnetic field. The parallel component is split into four hyperfine lines due to interaction with the copper nucleus ($I = 3/2$). The splitting of the four lines gives the parallel component of the anisotropic hyperfine interaction $A_{||} = 0.0137$ cm^{-1}. The $g_\perp$ component ($g = 2.07$) is the most intense line in the spectrum, and usually the $A_\perp$ hyperfine components are not clearly resolved.

In silicoaluminophosphate three methods of copper introduction have been explored. The most commonly used method is liquid state ion-exchange. In some systems solid-state ion-exchange is also successful. The location of the copper cations seems identical in both preparation methods and depends mainly on the hydration state or the interaction with adsorbates.[167] The third method of Cu(II) introduction is impregnation, which is especially useful if the molecular sieve has no formal ion-exchange capacity. In all systems the magnetic parameters of Cu(II) in the fresh state and the rehydrated state are almost identical, showing that the dehydration/rehydration cycle is fully reversible.

ESEM data analysis of adsorbed D_2O in SAPO-11 with a 10-ring channel shows interaction of four deuteriums (two water molecules) with the copper cation at a distance of 0.28 nm. Therefore Cu(II) is directly coordinated to three lattice oxygen atoms from a 6-ring window and two adsorbate molecules, producing a five-coordinated complex (Figure 17a). In SAPO-5 with a larger 12-ring channel, Cu(II) coordinates octahedrally to three oxygens and three water molecules (Figure 17b). After dehydration, the location of ion-exchanged Cu(II) in CuH-SAPO-5 and CuH-SAPO-11 is similar. The ESR and ESEM data suggest that Cu(II) is located at site I in a hexagonal prism. The important structural difference between SAPO-5 and SAPO-11 is that SAPO-5 has a circular 12-ring channel ($d = 0.73$ nm), whereas SAPO-11 has an elliptical 10-ring channel (0.63 by 0.39 nm). This results in different coordination numbers for H_2O as well as for NH_3 and methanol. Upon adsorption, Cu(II) migrates from a hexagonal prism (site I) to a site in a main channel (site II*).

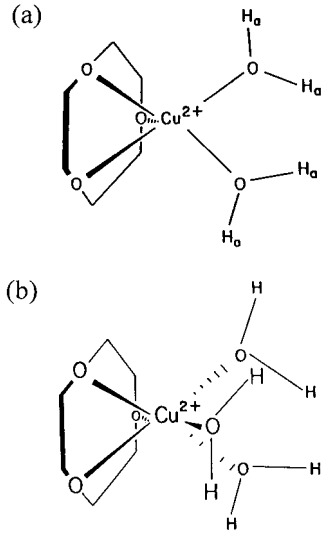

Figure 17. Schematic representation of Cu(II) coordinated to water in (a) CuH-SAPO-11 and (b) CuH-SAPO-5. (Reprinted with permission from refs 6 and 165. Copyright 1991 American Chemical Society.)

Cu(II) complexes with four ammonia molecules have predominantly square planar coordination.[167] ESEM data are typically less precise in this case due to the large quadrupolar moment of the nitrogen atom. Additionally, a significant amount of spin density is found on the nitrogen. Fortunately the number of coordinated ammonia molecules can be extracted from the resolved nitrogen superhyperfine splitting lines, where $(2m + 1)$ lines can be seen for *m* $^{14}NH_3$ molecules or $(m + 1)$ lines are seen for *m* $^{15}NH_3$ molecules. The square planar geometry, which is also indicated by the magnetic *g* parameters for copper-ammonia complexes, is well established in many zeolites.[170] In SAPO-11 Cu(II) is suggested to be located at the center of a double 10-ring (site U), coordinated to four molecules of ND_3. In SAPO-5 three $^{15}ND_3$ molecules are directly coordinated to Cu(II).

Methanol adsorption is an excellent example for determination of the local adsorption geometry by selective deuteration. Three-pulse ESEM signals recorded from samples with adsorbed CH_3OD and CD_3OH are simulated by neglecting the weak quadrupole moment of the ^2D nuclei. Fitting such ESEM

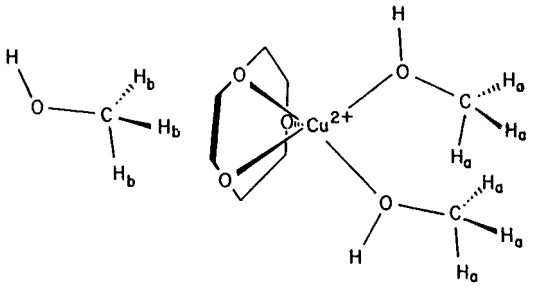

Figure 18. Schematic representation of Cu^{2+} coordinated to methanol in CuH-SAPO-11, showing direct coordination to two methanols and three lattice oxygens from the 6-ring window in the same 10-ring channel and indirect coordination to one methanol molecule in an adjacent 10-ring channel. From the ESEM data the distances of $Cu^{2+}-H_a$, $Cu^{2+}-H_b$, $Cu^{2+}-H_c$, and $Cu^{2+}-H_d$ are 0.40, 0.33, 0.43, and 0.28 nm, respectively. (Reprinted with permission from ref 6. Copyright 1991 American Chemical Society.)

data in SAPO materials often requires a two-shell model. The structure derived from the ESEM data is displayed in Figure 18. Two methanol molecules are directly coordinated to the copper center via their hydroxyl oxygens. A third molecule is indirectly coordinated to Cu(II) and likely hydrogen-bonded to the framework in an adjacent twelve-ring channel. These results are consistent with the known structural data of SAPO-5. In the case of SAPO-11 a similar coordination is suggested. The unusual pentacoordination of copper can be explained by the bulky size of the methanol molecule (Figure 18).[6]

The coordination of C_2D_4 to Cu^{2+} is determined by deuterium modulation. The ESR spectrum of a sample with adsorbed ethylene is almost the same as that of a dehydrated sample. ESEM analysis shows interaction with four equivalent deuteriums at a distance of 0.36 nm. This is consistent with a geometry where one ethylene molecule has its molecular plane perpendicular to a line toward Cu(II). There is information available about the exact location of the copper cation. Since the ethylene molecule is too large to enter a hexagonal prism through a 6-ring window, the Cu(II) location is close to a 10-ring channel. Therefore, ethylene adsorption most likely causes migration of Cu(II) from inaccessible site I in a hexagonal prism to a site II* or II, where interaction with ethylene can take place.

High-temperature solid-state ion exchange has been performed in H-SAPO-5 and H-SAPO-11 with various copper compounds such as CuF_2 and CuO. The ESR parameters of both hydrated and dehydrated samples depend only slightly on the method of copper introduction into the system. However, electron spin−echo modulation data show that the distances between Cu(II) and several adsorbates are shorter for solid-state ion-exchange than for liquid-state ion-exchanged samples by 0.02−0.04 nm. This was explained by a local structural distortion of the Cu(II) coordination environment by additional coordination of an anion from the copper source.[167]

Some attempts have been made to incorporate copper(II) into the framework of silicoaluminophosphates.[168,171,172] To attempt this, a copper salt is added to the synthesis gel. While Ragic et al.[171] report that copper addition to the gel actually inhibits the synthesis, Lee et al.[168] and Moen et al.[172] were able to synthesize H-SAPO-5 and H-SAPO-11. Nevertheless both groups conclude that Cu is not incorporated into the framework of these structures under the conditions prevailing in their synthesis. In the synthesis of SAPO-5 (reported by Moen and Nicholson[172]) copper(II) is believed to be reduced by the templating amines to copper (I), which subsequently disproportionates to metallic copper and copper(II). Calcination of this material produces a mixture of CuO and SAPO-5. Lee et al.[168] report on the basis of ESR and ESEM measurements that Cu(II) in synthesized nominal CuAPSO-11 is located in ion-exchange positions, which were previously also detected in CuH-SAPO-11 prepared by conventional liquid-state ion-exchange. In nominal CuAPO-11, Cu(II) is located in extraframework positions of AlPO-11. It was also concluded that the complexation of the cupric ions with the template during the synthesis may prevent successful incorporation of copper (II) into the framework. However, Munoz and co-workers[173] have recently reported a synthesis of CuAPO-5 in which Cu(II) was shown to be in a tetrahedral framework site.

Cu in SAPO-34

CuH-SAPO-34 can be prepared by liquid-state or solid-state ion-exchange. The ESR parameters of hydrated samples are characteristic of octahedrally coordinated Cu(II) complexes. Modulation from ^{27}Al was also observed, which indicates that the cupric ion is specifically associated with lattice aluminum. A complex $Cu(O_F)_3(H_2O)_3$, where O_F refers to a framework oxygen, is most likely. Site I seems to be the most likely site (see Figure 3) where a slightly distorted octahedral complex can exist. After dehydration two distinct Cu(II) species are detected.[174] By comparison to data of Cu(II) in CuNa−Y and CuCa−X, one species is assigned to be trigonally coordinated. This species is logically located near the plane of a 6-ring. This location has been identified by single-crystal X-ray diffraction for Cu(II) cations in dehydrated chabazite.[175] A possible location for the second species is in a hexagonal prism (site I). This location has been identified for Mn(II) in dehydrated Mn-chabazite.[176]

Adsorbate interactions studied by ESR reveal that one type of Cu(II) complex is observed with adsorption of water, ammonia, ethylene, dimethyl sulfoxide, ethanol, and 1-propanol while two different Cu(II) complexes are observed with the adsorption of methanol. From ESEM it was determined that Cu(II) interacts with three equivalent ammonia molecules, one ethylene molecule, and one molecule of dimethyl sulfoxide. Ammonia adsorption results in an octahedral complex in which the Cu(II) is coordinated to three zeolitic oxygens and to three ammonia molecules. Through ESEM spectroscopy the Cu(II) cation was determined to interact with three molecules of ethanol, two of which interact at a shorter distance than the third.[174] In a second study the results in CuH-SAPO-34 were compared to the structurally analogous aluminosilicate, chabazite.[177] The generation of two distinct Cu(II) species upon dehydration

was also detected in CuH chabazite. It was also discovered that Cu(II) cations in chabazite interact with the various adsorbate molecules in a similar manner as for Cu(II) cations in SAPO-34. Adsorption of methanol generates two distinct Cu(II) complexes in both molecular sieves, while the adsorption of ethanol and propanol generates only one Cu(II) complex. Differences, which are related to differing cation densities in these two materials, are observed in the interaction of Cu(II) with water, propanol, and ethylene.[177]

Both liquid-state ion-exchange of CuH-SAPO-34 and solid-state ion-exchange of H-SAPO-34 with CuO, $CuCl_2$, and CuF_2 were carried out. Except for slight differences, it was found that the location of the Cu(II) ions and the adsorbate interactions are the same for ion-exchange in aqueous solution and solid-state ion exchange.[174,177]

Cu in SAPO-37 and SAPO-42

Of potential interest are SAPO materials which are structurally analogous to zeolites such as SAPO-37 (analogous to zeolite X, Y) and SAPO-42 (analogous to zeolite A). Cu(II) locations and adsorbate interactions were studied in SAPO-37 which is difficult to handle due to its instability toward water at temperatures below 348 K.[3] Therefore, the Cu(II) species of fully hydrated CuH-SAPO-37 could not be investigated. Cu(II)−water complexes could be observed in the as-synthesized materials, which were ion-exchanged with NH_4^+ prior to exchange with Cu(II). The ESR parameters for these species are similar to those of a pentacoordinated Cu(II) species found in Cu−Na and CuK−SAPO-42.[179] The echo modulation parameters indicate two water molecules directly coordinated to the Cu(II) cation while three more distant water molecules are most likely adsorbed onto the molecular sieve walls. The combined ESR and ESEM data indicate a Cu(II) species pentacoordinated to three framework oxygens and two water ligands.

The adsorption of ammonia and pyridine generates a Cu(II) species which is coordinated to three adsorbate ligands. In contrast, when various cationic forms of zeolite X and Y are exposed to the same adsorbates the cupric cation is coordinated with four adsorbates in a square planar geometry.[170] The Cu(II) complex formed in SAPO-37 after the adsorption of ethanol and propanol is also different from that observed in zeolite X. The Cu(II) species generated in the SAPO material is tetrahedrally coordinated to three framework oxygens and one ethanol molecule, while in zeolite Y three ethanol molecules are coordinated to one cupric cation. However, some similarities also exist. Coordination to three methanol molecules and two dimethyl sulfoxide molecules is detected in both systems. In the later case the ESR parameters are not identical which indicates a subtlely different geometry of the complex.[178]

A further interesting system, which has been studied in detail is the comparison of zeolite A with isostructural SAPO-42.[180,181] In zeolite A the clear influence of monovalent and divalent cocations on the copper(II) location was documented. Various Cu(II) species formed after hydration, dehydration, and exposure to adsorbates were identified by ESR and ESEM spectroscopies. A pentacoordinated Cu(II) species was identified in hydrated CuM-SAPO-42 (M = Ca, Mg, Na, K). This species coordinating two water ligands and three framework oxygens is stable up to 373 K. In contrast, Cu(II) ions in rehydrated samples of CuNa-A and CuK-A are octahedrally coordinated to three water ligands. In a hydrated sample of CuRb−SAPO-42 the Cu(II) ion is tetrahedrally coordinated to three zeolitic oxygens and one water molecule. A similar coordination was reported for Cu(II) ions in CuRb-A zeolite.[181] The location of the above-described complexes is most likely near site SII* in the α-cage.

The adsorption of methanol also illustrates the influence of the cocation on the stereochemistry of the Cu(II) ion. The Cu(II) ions in CuMg− and CuCa−SAPO-42 were found to interact with two nonequivalent molecules of methanol. In contrast, the copper(II) ions in CuNa− and CuK−SAPO-42 interact with two equivalent methanol molecules forming a complex with rhombohedral symmetry, while CuRb−SAPO-42 with adsorbed methanol generates a trigonal-bipyramidal Cu(II) complex. Similarly, the stereochemistries of Cu(II) complexes formed after the adsorption of ethylene depend on the cocation present.[180] These studies suggest that both the size and the charge of the cocation influence the coordination of the Cu(II) ion with various adsorbates. The conclusions drawn from a comparison of copper complexes in divalent and monovalent cations containing SAPO-42 molecular sieves provide information useful for controlling the location of a catalytically active species on a SAPO-42 type surface.

Cupric Ions in Other Structure Types and Catalysis

Divalent copper ion-exchanged into SAPO-18 (AEI)[182] and SAPO-17 (ERI)[183] was used as a spin probe to examine its location in these molecular sieves and its interaction with small molecular adsorbates. Using ESR and ESEM spectroscopic methods it was shown that fully hydrated samples of Cu-SAPO-18 have Cu(II) in octahedral symmetry coordinated by six water molecules. Dehydration causes successive changes in the coordination geometry of Cu(II) and shifts its location toward a hexagonal window of the pear shaped supercage. This is confirmed by ^{31}P ESEM measurements which show that during dehydration Cu(II) decreases its distance from the hexagonal window plane from 0.36 to 0.17 nm which is a rather remarkable change in distance on dehydration.

SAPO-17 is a small pore molecular sieve with eight-membered ring pore openings. The structure of calcined SAPO-17 is analogous to the natural zeolite erionite. Polyhedral cages observed in SAPO-17 are double hexagonal prisms, cancrinite cages and erionite cages (supercages). In hydrated Cu-SAPO-17, Cu(II) ions exist as $Cu(H_2O)_6^{2+}$ and are located at sites inside the supercage. Upon thermal treatment, some of the Cu(II) ions migrate into the smaller cancrinite cages, which are not accessible to large molecules such as ethylene.

Cu(II) was also ion-exchanged into SiVPI-5 and SAPO-8 which were synthesized by a new method and which are large pore materials with 18- and 14-ring channels, respectively.[184] Evidence was reported for the incorporation of Si into the framework which enhances the ion-exchange capacity. ^{2}D ESEM was again used to determine the coordination geometry to water, ammonia, benzene, and pyridine. Weakly polar benzene does not coordinate directly to Cu(II) in SiVPI-5, but the more polar pyridine is able to induce Cu(II) migration from less accessible sites to the main channel where direct coordination occurs.

The reaction of copper salts with $AlPO_4$-5 or VAPO-5 has been investigated by Whittington and Anderson.[185] Ion incorporation is proposed to occur initially at defect sites, which gives rise to a number of unique environments upon Cu(II) incorporation as detected by ESR spectroscopy.

The interaction of nitric oxide with carbon monoxide on the surface of copper containing aluminophosphates and silicoaluminophosphates of the AFI structure was studied by a transient response technique.[186] In the temperature range studied (60−300 °C), the catalysts start to interact first with carbon monoxide. Cu/$AlPO_4$-5 and Cu/SAPO-5 exhibit activity toward the conversion of nitric oxide to nitrogen above 100 °C, which is comparable to a CuO/Al_2O_3 catalyst.

The catalytic activity of copper ion exchanged SAPO-5, SAPO-11, and SAPO-34 for selective reduction of NO with C_3H_6 under an oxidizing atmosphere has been tested by Ishihara et al.[187] Under the experimental conditions of their study, Cu-SAPO-34 exhibits higher activity for NO-reduction than Cu-ZSM-5 and sustains this catalytic activity up to 600 °C. While the catalytic activity of Cu-SAPO-11 is comparable to that of Cu-ZSM-5, the activity of Cu-SAPO-5 is significantly lower.

J. Zinc

Zinc is generally considered a good candidate for isomorphous substitution into the framework of aluminophosphates and silicoaluminophosphates. Framework incorporation has been claimed for several structure types including AFI,[188,189] AEL, ATS, AFR,[190] CHA,[191,192] AEI,[193] and AlPO-44.[194] The incorporation of zinc into aluminophosphate frameworks is generally difficult to prove and usually requires EXAFS data and/or Rietveld X-ray refinements. The parameters extracted from the Zn K-edge EXAFS spectra measured on powdered MnZnAPO-34 show a zinc atom coordinated with four oxygen neighbors at a distance of 0.194 nm in the first shell. According to these data, zinc atoms are isomorphously substituted in the molecular sieve framework.[191] It was stated that zinc substitutes for aluminum but this is not proved by the EXAFS data. Tusar et al.[192] have reported the synthesis of a pure phase zinc-rich ZnAPO-34 with 20% replacement of aluminum or phosphorus by zinc. EXAFS analysis shows that zinc is coordinated to four oxygens at a distance of 0.194 nm in as-synthesized ZnAPO-34 and to three oxygens at a distance of 0.196 nm in calcined ZnAPO-34. This decrease in the number of oxygen atoms coordinated to zinc is explained by eq 6.

$$(O)_2Zn(OH)_2 \rightarrow (O)_2Zn{=}O + H_2O \qquad (6)$$

The ^{31}P MAS NMR spectra of ZnAPO-34 show up to four signals, while the ^{31}P NMR spectrum of SAPO-34 shows only one line near −30 ppm resulting from tetrahedral phosphorus (P(4Al)). The various lines are attributed to different P(nAl, (4 − n)Me) units, although a band at −20 ppm can also be attributed to the presence of P−OH defect groups in ZnAPO-34. However, a calculation of the fraction of Zn in ZnAPO-34 after deconvolution of the spectra is in good agreement with chemical analysis. Therefore, this has been taken as evidence for framework incorporation of Zn into the SAPO-34 framework.[192, 195]

Elangowan et al.[196] found a considerable increase of the unit cell volume with introduction of $ZnSO_4$ into the synthesis gel for AlPO-5 and AlPO-11. Together with a shoulder in the ^{31}P MAS NMR spectra these hints were taken as evidence for the isomorphous substitution of zinc into the aluminophosphate framework. An increase in acidity of ZnAPO-11 and ZnAPO-5 compared to the parent materials is shown by temperature-programmed desorption of pyridine and is reflected in the catalytic transformation of camphene.[196] These samples with increased acidity exhibit an increase of camphene conversion and a decrease of tricyclene selectivity.

Large-pore zinc-incorporated ZnAPO-36 (ATS topology) was prepared and characterized by various techniques.[197] The surface composition determination by XPS analysis revealed that the concentrations of zinc and phosphorus are higher on the surface than in the bulk of the ZnAPO-36 catalyst. By XPS the observed binding energy of Zn $2p_{3/2}$ corresponds to that of Zn $2p_{3/2}$ in ZnO, but the site energy distribution in ZnAPO-36 is very broad. The larger number of strong acid sites compared with $AlPO_4$-5, SAPO-5 and MAPO-5 is reflected in significant catalytic activity in acid-catalyzed reactions such as cumene, toluene, and ethanol conversion reactions.

The catalytic transformation of 1-butene was studied by Escalante et al.[198] over ZnAPSO-11, impregnated Zn/SAPO-11, and unpromoted SAPO-11. The data indicate a higher skeletal isomerization selectivity for ZnAPSO-11 which is in agreement with a higher density of acid sites in this catalyst. The results were explained in terms of a model of Gielgens et al.[199] in which the substitution of Al(III) by Zn(II) ions leads to partially unsaturated Zn(II) ions in the vincinity of structural P−OH groups.

The synthesis of zinc-containing aluminophosphates with the FAU and AFR structures has been reported.[200,190] Several characterization techniques indicate that true framework incorporation of zinc occurs for the AFR structure. The isomerization of *m*-xylene was used as a model reaction to probe the catalytic activity of the AFR structure with zinc and confirm the presence of the Brønsted acid sites. The catalytic tests showed that the acid sites generated upon framework incorporation of Zn are stronger than those resulting from incorporation of Si into the AFR framework.[190]

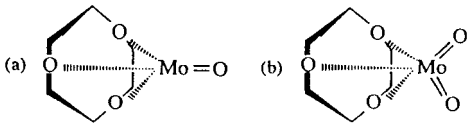

Figure 19. Possible oxomolybdenum species in SAPO-5 and SAPO-11 molecular sieves (a) monoxomolybdenum species and (b) dioxomolybdenum species. (Reprinted with permission from ref 202. Copyright 1993 American Chemical Society.)

K. Molybdenum

Molybdenum can be introduced into molecular sieves via solid-state ion-exchange using MoO_3. ESR experiments reveal that after solid-state ion-exchange and subsequent dehydration at 298 K, no signal due to Mo^{5+} is obtained.[201] Dehydration at elevated temperatures produces a weak ESR spectrum which is composed of two signals. The signals are ascribed to $Mo_{6c}(V)$ (compressed octahedral) and $Mo_{5c}(V)$ (square pyramidal) species where the subscripts denote coordination numbers. After dehydration the interaction with different adsorbates was investigated.[202] Upon adsorption of polar molecules (D_2O, methanol) a partial oxidation to molybdenum blue (a mixed valence Mo(V)−Mo(VI) oxide) is detected. Nonpolar molecules such as ethylene only interact with one of the two species showing that one species has a more recessed location.[202] From ESEM data and adsorbate interactions it is shown that Mo(V) exists as oxomolydenum ions as either $(MoO)^{3+}$ or $(MoO_2)^+$ (Figure 19). The $[Mo(V)O_2]^+$ species seems more likely due to the inability of SAPO materials to stabilize highly charged species. Oxidation may lead to oxidation of Mo(V) to Mo(VI) following eq 7.

$$Mo(V) + O_2 \rightarrow Mo(VI) + O_2^- \qquad (7)$$

This is indicated by an intensity loss of the Mo(V) ESR signal and the appearance of an O_2^- signal in the ESR spectrum. Hydrogen reduction and subsequent ammonia treatment produce a strong ESR signal, which is ascribed to a $Mo_{4c}(V)$ species with distorted tetrahedral coordination.

L. Platinum and Rhodium

Platinum

Platinum incorporation into aluminophosphate frameworks has not been reported so far, but some studies on characterization and catalytic testing of silicoaluminophosphates prepared by impregnation or ion-exchange have been published. A series of papers was published by Campelo et al. on hydrocracking and hydroisomerization of *n*-alkanes on bifunctional Pt/SAPO-5 and Pt/SAPO-11 catalysts.[203−205] These materials were prepared by impregnation of silicoaluminophosphates with $Pt(NH_3)_4Cl_2$ and subsequent reduction. The platinum loading was adjusted to 0.5 wt %. In studies with *n*-hexane,[204] *n*-heptane,[205,206] and *n*-octane[203] it was found that the size of the pores of the silicoaluminophosphate support can determine to large part the selectivity of hydroconversion. The differences in selectivity between Pt/SAPO-5 and Pt/SAPO-11 were explained by slower migration of alkenic intermediates in the channels of SAPO-11 and by steric constraints at the channel openings. The catalytic activity of *n*-alkanes increases with chain length because of the involvement of more stable carbenium ion intermediates. The selectivity for isomerization decreases with *n*-alkene chain length for Pt/SAPO-5 and increases for Pt/SAPO-11. In a subsequent study, *n*-octane and isooctane hydroconversion was investigated to determine the influence of channel size on the activity and selectivity.[207] It was found that the reaction schemes for *n*-octane and isooctane transformation are not the same due to different channel sizes in the SAPOs studied. The channel sizes as well as the size and the shape of the space available near the acid centers determine the selectivity of *n*-octane and isooctane isomerization and cracking on Pt-containing bifunctional catalysts.[207]

The conversion of *n*-heptane and *n*-hexane over Pt/SAPO-11 was investigated by Butt et al.[206,206] The reaction pathways were found to be similar on SAPO-11. With incorporation of sodium a pronounced formation of aromatics was detected. The bifunctional nature of the catalyst was reflected in the difference in activity versus constant selectivity for cracking and isomerization.

High selectivity for *n*-octane isomerization has been observed on medium-pore Pt/SAPO-11, -31, and -41, while preferential hydrocracking has been found for large pore Pt/SAPO-5.[208] Isomerization products consist of monobranched isomers with a negligible amount of dibranched isomers. The isomerization selectivity decreases in the order SAPO-41 > SAPO-31 > SAPO-11. The differences in selectivity were explained by diffusional restrictions and steric constraints.

A new molecular sieve process using Pt/SAPO-11 for lube dewaxing by wax isomerization was described by Miller.[210] Pt/SAPO-11 shows both a high selectivity for wax isomerization and a low selectivity for secondary hydrocracking. Moderate acid activity and the one-dimensional nature of the 10-ring pores appear to contribute to its performance. However, much of the catalysis occurs at or near the external surface of the molecular sieve.

Rhodium

The adsorption of CO on Rh/SAPO-5, which was prepared by ion-exchange of SAPO-5 with $Rh(Cl)_3$ and subsequent hydrogen reduction, has been monitored by infrared spectroscopy.[211] The formation of a high-frequency dicarbonyl species was observed, as has been noted before for molecular sieve supported rhodium. This species was related to the presence of oxygen rather than water as was previously suggested. The authors propose that this dicarbonyl species acts as a neutralizing cation for the anionic SAPO-5 structure.

M. Silver

Silver ionic clusters and silver alcohol adducts are stabilized in γ-irradiated AgH-SAPO-5 and AgH-SAPO-11 molecular sieves at 77 K, where Ag(I) is

introduced by ion-exchange.[212] In dehydrated samples silver ionic clusters are not stabilized in contrast to several zeolites.[213] But after exposure to alcohols (methanol, ethanol, propanol) prior to irradiation, the clusters Ag_2^+ and Ag_3^{2+} are efficiently stabilized as demonstrated by ESR and ESEM spectroscopy.[212] Besides silver clusters, the formation of organosilver radicals such as $Ag^{\bullet}CH_2OH^+$ are observed. Analysis of the ESEM spectra show that organosilver radicals are located in 10-ring channels of AgH-SAPO-11 and 12-ring channels of AgH-SAPO-5 and are coordinated by two nonequivalent methanol molecules. The cluster Ag_2^+ is located in a 6-ring channel of both structure types and is stabilized through interaction with methanol molecules. The higher yield and stability of Ag_2^+ in SAPO-11 is associated with the preferential location of Ag(I) cations in adjacent 6-ring channels.

Electron spin resonance and electron spin−echo modulation have also been used to study paramagnetic silver species produced by γ-irradiation of AgH-SAPO-42. The results of the study were compared to the results reported earlier for isostructural AgNa-A zeolite.[214,215] Michalik et al.[214,215] found that in dehydrated AgH-SAPO-42 small silver clusters such as Ag_2^+ and Ag_3^{2+} are formed with very low yield, whereas in AgNa-A, Ag_3^{2+}, or Ag_6^{n+} are efficiently stabilized. It was postulated that there are different preferential locations of Ag(I) in A zeolite (SII′ in the β-cage) and in SAPO-42 (SII* in the α-cage). A greater mobility of Ag(0) in SAPO-42 compared to A zeolite due to a lower cation capacity in SAPO-42 is responsible for the observed differences. The differences between the two systems are less significant when γ-irradiation is carried out in the presence of adsorbates. In the presence of methanol, silver methoxy radicals are the major paramagnetic products of radiolysis in both AgNa-A and AgH-SAPO-42. ^{2}D and ^{27}Al ESEM results showed that, although $Ag^{\bullet}CH_2OH^+$ radicals are located in the α-cage in both systems, in AgNa-A they are closer to the zeolite framework. Such a location allows a more direct coordination of the radical to the framework nuclei with a partial shift of spin density away from the silver nucleus. In the presence of methanol both molecular sieves stabilize different clusters. Tetrameric species Ag_4^{n+} are stabilized in the α-cage of SAPO-42, while Ag^{2+} is trapped in the β-cages of zeolite A.[216,67] It was postulated that the agglomeration process is affected by differences in the preferential locations of Ag^+ in both molecular sieves due to the different cation densities. In the presence of ammonia a silver species $Ag{\cdot}NH_3$ is formed in both systems, while in AgH-SAPO-42 Ag interacts additionally with two more distant ammonia molecules. This might be explained by a more central location for this species in the α-cage of SAPO-42 in comparison to zeolite A.

N. Zirconium

The addition of zirconium to the synthesis gel of SAPO-11 has been reported by Mériaudeau et al.[217] Zirconium is not incorporated into the SAPO-11 framework but is localized, at least partially, in the pores of the material. When used in *n*-butene isomerization, Zr-SAPO-11 exhibited a higher isobutene selectivity compared with SAPO-11. The improved isobutene selectivity is attributed by Mériaudeau et al. to the presence of zirconium in the pores inducing partial blocking and, therefore, causing increased shape selectivity. In addition, a very small number of external sites of Zr-SAPO-11 might explain the improvement in isobutene selectivity and the stability with time on stream found in that study.

Table 9. Catalytic Efficiency of Pd(I) and Ni(I) Containing SAPO-5, SAPO-11 and SAPO-34 (Batch, 400 hPa Ethylene)

sample	*T*/K	activity/%	selectivity/%
H-SAPO-*n*	80 100	0.1	
PdH-SAPO-11	100	2.5	<50
PdH-SAPO-5	100	9.3	<20
NiH-SAPO-34	80	0	
NiH-SAPO-11	80	4.74	76
NiH-SAPO-5	80	6.12	21
NiAPSO-11	80	3.05	93
NiAPSO-5	80	6.99	74

IV. Catalysis

A. Ethylene Dimerization by Nickel(I) and Palladium(I)

In the previous sections it was shown that a great deal has been learned about the control of cation location and the geometry of adsorbate interactions of metal ions such as nickel(I) and palladium(I) by detailed ESR and ESEM studies. The long-range goal of such work is to relate this structural control to catalytic efficiency and guide the development of new catalysts. Initial studies of ethylene dimerization, which is catalyzed by nickel(I) and palladium(I) have been carried out to demonstrate this approach.[218−220] The reaction can be discussed in two steps,[221] in which the first step is dimerization to 1-butene as shown in eq 8.

$$2C_2H_4 \xrightarrow{\text{Pd(I), Ni(I)}} \text{1-butene} \qquad (8)$$

The subsequent second step of 1-butene isomerization is an equilibrium reaction with predominant formation of *cis*- and *trans*-2-butene on acidic catalysts.[222] Analysis of the butenes and several side products as well as the loss of ethylene was measured by gas chromatography. Studies demonstrate that the process is indeed catalyzed by nickel(I) or palladium(I) which have been detected by ESR spectroscopy under conditions showing enhancement of the catalytic efficiency (Table 9).[218−220]

ESR and ESEM spectroscopy allow a more detailed investigation of the reaction on a molecular level. After the adsorption of ethylene a π-bonded Ni(I)− or Pd(I)−ethylene complex is obtained. In most cases the active center is coordinated to one ethylene molecule at a distance of about 0.35 nm (Figure 20). Under reaction conditions the ESR spectra change and new species are detected, which can be attributed to Ni(I)−butene complexes. The same complexes were

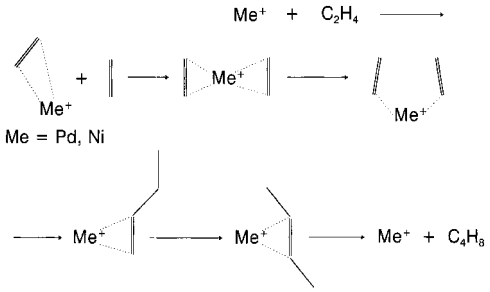

Figure 20. Schematic reaction sequence for Pd(I) and Ni(I) catalysis of the dimerization of ethylene.

obtained by *n*-butene adsorption on activated samples and therefore their assignment is unambiguous. Additionally, ESEM analysis shows interaction with eight deuteriums at different distances.[219] Butene complexes were not obtained in PdH-SAPO-34 and NiH-SAPO-34, which shows that due to the smaller channel size no reaction at temperatures below 100 °C occurs.[219]

B. Oxidation Reactions

In the continual effort to transform fine chemical production into more environmentally benign technologies, metal-containing aluminophosphate molecular sieves offer tremendous potential as catalysts for heterogeneous oxidation in the production of these chemicals. This follows from the significant advancement in the field of heterogeneous catalysis by molecular sieves following the success of titanium-containing silicalite (TS-1). Substitution of metal cations with redox properties such as Fe, Co, Mn, and V into aluminophosphates may be expected to afford novel heterogeneous catalysts for liquid-phase oxidation reactions (Table 10).

Sheldon and co-workers found that CoAPO-11 and CoAPO-5 are both effective, stable and recyclable solid catalysts for the facile oxidation with O_2 of *p*-cresol to *p*-hydroxybenzaldehyde at 50 °C with conversion and selectivity both reaching 90%.[223,224] The superior performance of the catalysts over homogeneous cobalt salts was attributed to the fact that unlike the cobalt salt, CoAPOs cannot form μ-hydroxo-bridged cobalt dimers. In other reports, Lin et al.[225] showed CoAPO-5 to be an active catalyst for the auto-oxidation of cyclohexane to acetic acid. At 30−40% conversion, selectivity to adipic acid was up to 45%. The oxidation of saturated hydrocarbons involving CoAPO molecular sieves has been demonstrated by Krausshaar-Czarnetzki et al.[112] The redox properties of the catalyst were interpreted in terms of the ability of framework Co to change between Co(II) and Co(III) oxidation states. However, as discussed earlier this conversion is controversial.

The autoxidation of cyclohexane at low conversions to obtain cyclohexanol and cyclohexane was investigated by Vanoppen et al. using CoAPO-5 and CoAPO-11 molecular sieves.[226] For CoAPO-5, cyclohexyl hydroperoxide is the main product (Figure 21), which is easily converted into monofunctional oxidation products. CoAPO-11 is catalytically more active than CoAPO-5 despite the lower channel diameter of CoAPO-11 which should hinder diffusion of the products. These catalytic results have been ascribed to a higher dispersion of cobalt in CoAPO-11.

Among the products of liquid-phase oxidation of cyclohexene, adipic acid is the most important. Industrially, adipic acid is produced via two-step liquid-phase oxidation of cyclohexene with air and nitric acid as oxidant. To increase the yield of adipic acid in a environmentally friendly one-step process most studies favor the oxidation of cyclohexane (Figure 21). CoAPO-5 has been found to be a potential catalyst for one-step liquid-phase oxidation of cyclohexene to produce cyclohexanone and adipic acid without any promoter being added and with no induction period.[221] The study shows that high cyclohexene concentration, a high reaction temperature and high oxygen pressure with a reaction time of 3−4 h will result in a high yield of adipic acid. A 45% yield of adipic acid can be obtained when the conversion of cyclohexene is about 50% after 3 h of time on stream.

Sheldon and co-workers also investigated the catalytic behavior of a variety of redox MeAPOs in liquid-phase oxidations with O_2 and tetrabutylhydroperoxide (TBHP). Examples include the oxidation of alkanes and alkylaromatic alcohols and the epoxidation or oxidative cleavage of olefins with TBHP. They reported for example that CrAPO-5 is an excellent and recyclable catalyst for the oxidation of secondary alcohols to the corresponding ketones using TBHP or O_2 as the oxidant.[228] Chen et al. reported that CrAPO-5 was an active, stable, and selective catalyst in the decomposition of cyclohexyl hydroperoxide toward cyclohexanone, benzylic oxidations and the oxidation of secondary alcohols with TBHP and O_2.[229,330] VAPO-5 and VAPO-11 were both demonstrated by other researchers to catalyze oxidations, such as epoxidation of allylic alcohols analogous to homogeneous vanadium salts[25,231] and benzylic oxidations with TBHP and oxygen.[25]

The stability of VAPO-5 as a catalyst for the epoxidation of 3-phenyl-2-propen-1-ol and the oxidation of 3-octanol by TBHP has been investigated by Haanepen et al.[232] They concluded that VAPOs are not suitable catalysts for oxidation reactions in the liquid state where it is desired to improve the selectivity of the reaction by means of the pore structure. In an early stage of the reaction small amounts of vanadium are extracted from the framework. The amount depends on the substrate and the reaction conditions. These vanadium ions in solution contribute largely to the observed activity. Thereafter, the leaching of vanadium stops due to strong sorption of molecules into the micropores of VAPO-5, which makes most vanadium sites inaccessible for reaction and leaching.

The catalytic activities of MeAPO-11 (Me = Fe, Co, Mn) for the hydroxylation of phenol with hydrogen peroxide have been examined by Dai et al.[233] They demonstrated that MeAPOs have significant catalytic activities for this reaction and that introduction of these metals significantly improves the levels of conversion. FeAPO-11 shows comparable performance to TS-1. The activity depends on the Al/Fe ratio and the level of acidity of the molecular sieves.

Table 10. Survey of Oxidation Reactions Tested with Aluminophosphate Based Catalysts

substrate	desired product(s)	oxidant	catalyst(s)	*T*/K	conversion (selectivity)/%		ref
ethane	ethene	O_2	VAPO-5	973	17.1	(46.8)	238
			CoAPO-5		16.5	(52.7)	
			CoVAPO-5		43.9	(40.8)	
ethane	ethene	air	MnAPO-5	723	1.38	(0.76)	237
propane	propene	O_2	VAPO-5	773	18.5	(91)	236
phenol	hydroquinone	H_2O_2	FeAPO-11	353 (3 h)	25.1	(49.3)	233
	catechol					(50.7)	
phenol	hydroquinone	H_2O_2	CoAPO-11	353 (3 h)	25.5	(44)	233
	catechol					(56)	
phenol	hydroquinone	H_2O_2	CrAPO-11	353 (3 h)	28.7	(17.0)	51
	catechol					(10.8)	
phenol	hydroquinone	H_2O_2	TAPSO-11	353 (3 h)	32.2	(21.3)	17
	catechol					(10.5)	
toluene	benzoic acid	TBHP[a]	VAPO-5	343 (22 h)	13	(78)	25
tolune	benzoic acid	TBHP	VAPO-31	303 (22 h)	44	(65)	29
ethene	ethene epoxide	TBHP	VAPO-5	343 (6 h)	51	(91)	25
cyclohexene	cyclohexene epoxide	TBHP	TAPSO-5	343 (6 h)	16.2	(79.0)	15
cyclohexanol	cyclohexanone	TBHP	CrAPO-5	358 (12 h)	72	(85)	229
		O_2		383 (19 h)	30	(97)	
α-ethylbenzyl alcohol	propiophenone	TBHP	CrAPO-5	358 (12 h)	77	(100)	229
		O_2		383 (19 h)	38	(90)	
cyclohexane	cyclohexanone	O_2	CrAPO-5	403 (1.4 h)	3.4	(71.0)	54
	cyclohexanol					(8.0)	
ethylbenzene	acetophenone	O_2	CrAPO-5	403 (6 h)	3	(42)	54
	ethylbenzene hydroperoxide					(58)	
toluene	benzonitrile	air/NH_3	VSAPO-37	773	29.8	(28.7)	258

[a] Tetrabutylhydroperoxide.

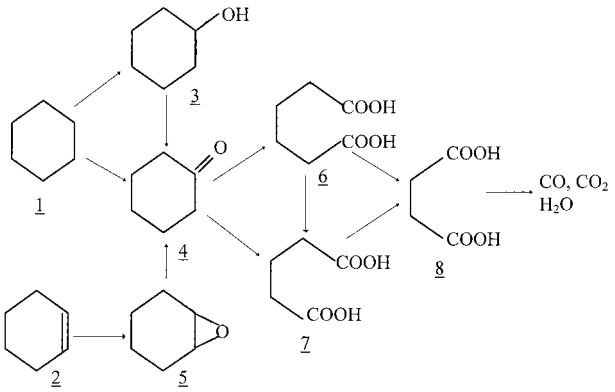

Figure 21. Main products and byproducts of cyclohexane (**1**) and cyclohexene (**2**) oxidation to yield cyclohexanol (**3**), cyclohexanone (**4**), cyclohexenoxide (**5**), adipic acid (**6**), glutaric acid (**7**), and succinic acid (**8**).

Medium-pore MeAPOs are more active than their larger pore counterparts. However, the external surface of the catalyst was found to have a significant role on their catalytic activity.

The oxidative dehydrogenation of alkanes, which is one of the important routes to obtain alkenes, has been tested by some researchers using vanadium-containing aluminophosphates.[36,234−236] VAPO-5 is active and selective for the oxidative dehydrogenation of propane. The catalytic properties of VAPO-5 are better than the corresponding AlPO-5 supported vanadium catalysts. Isolated tetrahedral V(V) species in the framework of AFI structure are proposed to be active sites for this reaction.[36,236]

The manganese-substituted molecular sieve MnAPO-5 was found to be an active catalyst for ethane dehydrogenation to produce ethene.[237] Good crystallinity was found to be essential for the MnAPO-5 catalyst to have unique properties, because the occlusion of manganese oxide particles in the channels or a collapse of the structure upon calcination have been found to decrease the ethene selectivity.[237] The presence of Mg(II) and V(V) species in vanadium−magnesium aluminophosphate MgVAPO-5 results in a more selective catalyst for the oxidative dehydrogenation of ethane.[236] The authors relate the catalytic properties of MgVAPO-5 to the presence of acid sites (Mg(II)) near redox sites (V(V)) in the molecular sieve framework. CoVAPO-5 was even more active than MgVAPO-5 (44% conversion compared to 8%), suggesting that the redox properties of cobalt are responsible for the observed activity. Recent results of the same group show that the activity for oxidative dehydrogenation of ethane decreases in the order CoVAPO-5 > VAPO-5 > CoAPO-5 > MgVAPO-5 while for the oxidation of cyclohexane it increases in the order MgVAPO-5 < CoVAPO-5 < VAPO-5 < CoAPO-5.[238]

TAPSO-5 has been used as a catalyst for the liquid-phase epoxidation of cyclohexene.[15,16] When H_2O_2 is used as the oxidant the formation of 1,2-cyclohexanediol is observed, which is a result of ring opening that may be catalyzed by the acid sites of the framework. When *tert*-butyl hydroperoxide is used as the oxidant, the epoxide is formed very selectively. Only traces of other products such as cyclohexenone, the diol and bicyclohexenyl are detected. Such a high selectivity for the epoxide has already been reported by Rigutto and van Bekkum[25] for the epoxidation of cyclohexene over VAPO-5 materials.

Direct hydroxylation of phenol yielding catechol and hydroquinone is observed over TAPO-5 and TAPO-11 catalysts.[17] Hydroxylation occurs to the extent of 32.2 and 17.7% for TAPSO-5 and TAPSO-11, respectively. The catalyic hydroxylation of TA-

PO-*n* molecular sieves is comparable to that of TS-1[239] and therefore suggests that titanium substitution into the framework of these molecular sieves is possible.

C. Methanol Conversion

The demand for olefinic feedstocks has increased rapidly in the past few years due to increased needs for synthetic fibers, plastics, and petrochemicals. The increase in demand for small olefins has periodically caused a shortage of the basic raw materials either because of a limitation in the present olefinic feedstock of suitable quality or a limitation in the present olefinic production capacity. Thus, alternative sources of ethene from nonpetroleum sources are required to keep pace with the demand for ethene and other olefins.

H-SAPO-34 (CHA structure) is acknowledged to be a powerful catalyst, with attractive performance in converting methanol to light alkenes, principally ethene, propene, and butene (MTO-process). However, the distribution among C_2, C_3 and C_4 alkenes was roughly comparable.[240] SAPO-18 (AEI structure) is a chabazite-related structure and comparable to SAPO-34 in activity and selectivity. The conversion of methanol to hydrocarbons can reach 100%, and the optimum distribution of ethene and propene in the hydrocarbon product can reach 80%. The catalytic activity of SAPO-34, which has roughly twice as many Brønsted acid sites as good quality SAPO-18, drops more rapidly than for SAPO-18.[241] For further improvement, transition metal substituted aluminophosphates such as (MeAPSO-34 and MeAPO-18) have been tested by several groups.[242−246] Inui et al.[242] and Thomas et al.[243] reported independently that nickel-containing SAPO-34 is one of the best catalysts for methanol to olefin (MTO) conversion yielding close to 90% ethene at almost 100% conversion at a reaction temperature of 450 °C. The catalytic performance was maintained at this temperature for 13 h; during this time no significant change in methanol conversion or ethene selectivity was observed. In contrast, NiAPO-18, which has a similar framework structure, is one of the poorest catalysts for the MTO reaction.[245] ZnAPO-18, CoAPO-18, and MgAPO-18 are all very reactive at temperatures above 350 °C.[246] The lower ethene selectivity and higher propene and butene selectivity of the Mg-, Co-, and ZnAPO-18 catalysts is also obtained with MeAPO-34 materials.[246] It is therefore suggested that the nature of the substituting element is more important than the difference in pore geometry between the AEI and CHA structures. Several authors investigated the correlation between the Brønsted acidity of the samples and their methanol conversion activity.[247,248] Besides selecting a molecular sieve with a different topology, the most straightforward way to change the acid strength and concentration of acid sites is by isomorphous substitution of elements having different atomic electronegativities, concentration, and distribution in the framework of the molecular sieve. Hocevar et al.[244,249,250] investigated MeAPSO-34 and MeAPSO-44 molecular sieves with Me = Co, Mn, Cr. They showed that introduction of transition metal ions influences the acid strength of MeAPSO-34 and MeAPSO-44 and consequently the selectivity toward ethene formation, which follows the Irving−Williams transition metal−ligand complex stability order. This order is a consequence of extra crystal field stabilization energy of the atomic d-orbitals compared to the ligation energy. If the ligation energy of ethene (π-complex) with a transition metal is higher, it will be less prone to subsequent oligmerization and, consequently, such a catalyst is more selective for ethene. If this model holds true, then Ni-containing samples should be the most selective ones for ethene, since Ni complexes have the highest crystal field stabilization energy. This was observed at least for NiAPSO-34.[240,243]

Some larger topologies such as AFI and ATS have been tested by Lischke et al.[251] and Akolekar.[197] The best catalytic results for the formation of lower olefins were achieved with NiAPO-5 which contains a relatively high density of Brønsted sites of moderate strength and a comparatively small portion of strong Lewis sites. However, on molecular sieves with 12-ring pores such as NiAPO-5 and ZnAPO-36 ethene and propene selectivity is low compared to the materials with a CHA topology and aromatic formation takes place to a considerable extent [197,251]

V. Conclusions and Outlook

The introduction of transition metal ions into silicoaluminophosphates can be achieved by liquid state or solid state ion-exchange, by impregnation, or by addition to the synthesis gel. The interesting question of whether various metal ions can be incorporated into the tetrahedral framework of SAPO-*n* or AlPO-*n* materials can be successfully addressed by the use of complementary techniques including DRS, IR, ESR and ESEM, NMR, Mössbauer spectroscopy, and EXAFS. It is also possible to characterize redox processes involving paramagnetic and nonparamagnetic oxidation states of a transition metal ion in aluminophosphate materials. However, the future use of in-situ techniques such as NMR and IR spectroscopies might lead to advanced understanding of aluminophosphate and silicoaluminophosphate based catalysts under “working conditions”.

The long-range significance of the spectroscopic studies described is to relate information about the metal species location and adsorbate geometry to the efficiency of specific catalytic reactions. Initial studies of this type on ethylene dimerization by nickel(I) or palladium(I) ions in SAPO-5, -11, and -34 have demonstrated the potential achievability of this goal. More detailed studies of this type should lead to improved understanding of catalysis by metal species on surfaces and in microporous materials on a molecular level. Extensive knowledge of the geometrical and structural factors affecting catalytic reactions can lead to the design of novel and improved catalysts.

It has been shown that transition metal ion containing AlPOs and SAPOs are interesting catalysts for a variety of heterogeneously catalyzed reactions such as oxidations. Although improvements have

been made for some catalytic systems, only two are close to being realized commercially. UOP and Norsk Hydro have built a pilot plant for the conversion of methanol into lower olefins using a SAPO-34 based catalyst. Chevron is working on an isodewaxing unit using Pt/SAPO-11. With two large-scale applications on the horizon, new processes might emerge when further improvements on the catalyst systems based on transition metal ion containing aluminophosphates and silicoaluminophosphates are made. However, the major problems of leaching of metal ions into solution[260] and pore blocking by the formation of bulky products[232] also need to be addressed for practical industrial application.

A new and growing field is the use of transition metal ion containing SAPOs and AlPOs as advanced materials such as capacitance-type chemical sensors as demonstrated by Balkus et al.[252] Aluminophosphate-based molecular sieves represent suitable host systems for the accommodation of polarizable molecules. The applicability of dye-loaded AlPO-5 for second harmonic generation based on an organized arrangement of molecular dipoles and for persistent spectral hole burning has been summarized by Schulz-Ekloff.[253] More research work is expected to expand into this area.

VI. Acknowledgments

This work has been generously supported by the U.S. National Science Foundation and the Robert A. Welch Foundation. We also have benefited from support from the Texas Advanced Research Program and the University of Houston Energy Laboratory. M.H. thanks the Deutsche Forschungsgemeinschaft for support.

VII. References

(1) Wilson, S. T.; Lok, B. M.; Messina, C. A.; Cannan, E. R.; Flanigen, E. M. *J. Am. Chem. Soc.* **1982**, *104*, 1146.
(2) Davis, M. E.; Saldarriaga, C.; Montes, C.; Garces, J.; Crowder, C. *Nature* **1988**, *331*, 698.
(3) Lok, B. M.; Messina, C. A.; Patton, R. L.; Gajek, R. T.; Cannan, T. R.; Flanigen, E. M. *J. Am. Chem. Soc.* **1984**, *106*, 6092.
(4) Flanigen, E. M.; Patton, R. L.; Wilson, S. T. In *Innovation in Zeolite Materials Science*; Studies in Surface Science and Catalysis; Grobet, P. J., Mortier, W. J., Vansant, E. F., Schulz-Ekloff, G., Eds.; Elsevier: Amsterdam, 1988; Vol. 37, p 13.
(5) Flanigen, E. M.; Lok, B. M.; Patton, R. L.; Wilson, S. T. In *New Developments in Zeolite Science and Technology*; Proceedings of the 7th International Zeolite Conference, Tokyo 1986; Murakami, Y., Iijima, A., Ward, J. W., Eds.; Kodansha Ltd.: Tokyo; Elsevier Science Publishers: Amsterdam, 1986; p 103.
(6) Lee, C. W.; Chen, X.; Kevan, L. *J. Phys. Chem.* **1991**, *95*, 8626.
(7) Calligaris, M.; Nordin, G. *Zeolites* **1982**, *2*, 200.
(8) Ashtekar, S.; Barrie, P.; Hargreaves, M.; Gladden, L. F. *Angew. Chem.* **1997**, *109*, 919.
(9) Hunger, M. *Catal. Rev. Sci. Eng.* **1997**, *39*, 345.
(10) Kevan, L. In *Time Domain Electron Spin Resonance*; Kevan, L., Schwartz, R. N., Eds., Wiley-Interscience: New York, 1979; p 279.
(11) Ichikawa, T.; Kevan, L.; Bowman, M. K.; Dikanov, S. A.; Tsvetkov, Y. D. *J. Chem. Phys.* **1979**, *71*, 1167.
(12) Kevan, L. *J. Phys. Chem.* **1981**, *85*, 1628.
(13) (a) Mims, W. B. *Phys. Rev.* B **1972**, *5*, 2409. (b) Mims, W. B. *Phys. Rev.* B **1972**, *6*, 3543.
(14) Dikanov, S. A.; Shubin, A. A.; Parmon, V. N. *J. Magn. Reson.* **1981**, *42*, 474.
(15) Tuel, A. *Zeolites* **1995**, *15*, 228.
(16) Tuel, A.; Ben Taarit, Y. *J. Chem. Soc., Chem. Commun.* **1994**, 1667.
(17) Ulagappan, N.; Krishnasamy, V. *J. Chem. Soc., Chem. Commun.* **1995**, 373.
(18) Zahedi-Niaki, M. H.; Joshi, P. N.; Kaliaguine, S. In *Progress in Zeolite and Microporous Materials*, Studies in Surface Science and Catalysis; Chon, H., Ihm, S.-K., Uh, Y. S., Eds., Elsevier: Amsterdam, 1996; Vol. 105, p 1013.
(19) Zahedi-Niaki, M. H.; Joshi, P. N.; Kaliaguine, S. *Chem. Commun.* **1996**, 47.
(20) Flanigen, E. M.; Patton, R. L.; Wilson, S. T. In *Innovation of Zeolite Materials Science*; Studies in Surface Science and Catalysis; Grobet, P. J., Mortier, W. J., Vasant, E. F., Schulz-Ekloff, G., Eds.; Elsevier: Amsterdam, 1988; Vol. 37, p 313.
(21) Camblor, M. A.; Corma, A.; Perez-Parenté *J. Chem. Soc., Chem. Commun.* **1993**, 557.
(22) Prakash, A. M.; Kurshev, V.; Kevan, L. *J. Phys. Chem. B* **1997**, *101*, 9794.
(23) Rigutto, M. S.; van Bekkum, H. *Appl. Catal.* **1991**, *68*, L1.
(24) Jhung, S. H.; Uh, Y. S.; Chon, H. *Appl. Catal.* **1990**, *62*, 61.
(25) Rigutto, M. S.; van Bekkum, H. *J. Mol. Catal.* **1993**, *81*, 77.
(26) Whittington, B. I.; Anderson, J. R. *J. Phys. Chem.* **1993**, *97*, 1032.
(27) Montes, C.; Davis, M. E.; Murray, B.; Narayana, M. *J. Phys. Chem.* **1990**, *94*, 6431.
(28) Flanigen, E. M.; Lok, B. M. T.; Patton, L.; Wilson, S. T. US Patent 4 759 919, 1988.
(29) Venkatarhri, N.; Hedge, S. G.; Sivasanker, S. *J. Chem. Soc., Chem. Commun.* **1995**, 151.
(30) Song, M. K.; Yeom, S. H.; Kim, S. J.; Uh, Y. S. *Appl. Catal. A* **1993**, *102*, 93.
(31) Chao, K. J.; Wu, C. N.; Chang, H.; Lee, L. J.; Hu, S. H. *J. Chem. Phys. B* **1997**, *101*, 6341.
(32) Chaudhari, K.; Das, T. K.; Chandwadkar, A. J.; Chandwadkar, J. G.; Sivasanker, S. In *Progress in Zeolite and Microporous Materials*, Studies in Surface Science and Catalysis; Chon, H., Ihm, S.-K., Uh, Y. S., Eds.; Elsevier: Amsterdam, 1996; Vol. 105, p 253.
(33) Kulkarni, S. J.; Rao, R. R.; Subrahmanyam, M.; Farsinavis, S.; Rao, P. K.; Rao, R. A. V. In *Zeolite Science 1994: Recent Progress and Discussions*; Studies in Surface Science and Catalysis; Karge, H. G., Weitkamp, J., Eds.; Elsevier: Amsterdam, 1995; Vol. 98, p 161.
(34) Weckhuysen, B. M.; Vannijvel, I. P.; Schoonheydt, R. A. *Zeolites* **1995**, *15*, 482.
(35) Lohse, U.; Brückner, A.; Kintscher, K.; Parlitz, B.; Schreier, E. *J. Chem. Soc., Faraday Trans.* **1995**, *91*, 1173.
(36) Blasco, T.; Concepcion, P.; López Nieto, J. M.; Pérez-Pariente, J. *J. Catal.* **1995**, *152*, 1.
(37) Singh, P. S.; Bandyopadhyay, R.; Rao, B. S. *J. Mol. Catal. A.* **1995**, *104*, 103.
(38) Escalante, D.; Giraldo, L.; Pinto, M.; Pfaff, C.; Sazo, V.; Matjushin, M.; Méndez, B.; López, C. M.; Machado, F. J.; Goldwasser, J.; Ramírez de Agudelo, M. M. *J. Catal.* **1997**, *169*, 176.
(39) West, A. R. *Basic Solid State Chemistry*; Wiley: Chichester, 1988.
(40) Demuth, D.; Unger, K. K.; Schüth, F.; Stucky, G. D.; Srdanov, V. I. *Adv. Mater.* **1994**, *6*, 931.
(41) Demuth, D.; Unger, K. K.; Schüth, F.; Srdanov, V. I.; Stucky, G. D. *J. Phys. Chem.* **1995**, *99*, 479.
(42) Radaev, S. F.; Joswig, W.; Baur, W. H. *J. Mater. Chem.* **1996**, *6*, 1413.
(43) Thiele, S.; Hoffmann, K.; Vetter, R.; Marlow, F.; Radaev, S. *Zeolites* **1997**, *19*, 190.
(44) Helliwell, M.; Kaucic, V. *Acta Crystallogr.* **1993**, *B49*, 413.
(45) Weckhuysen, B. M.; Schoonheydt, R. A. *Zeolites* **1994**, *14*, 360.
(46) Weckhuysen, B. M.; Schoonheydt, R. A. In *Zeolites and Related Microporous Materials: State of the Art 1994*; Studies in Surface Science and Catalysis; Weitkamp, J., Karge, H. G., Pfeiffer, H., Hölderich, W., Eds.; Elsevier: Amsterdam, 1994; Vol. 84, p 965.
(47) Weckhuysen, B. M.; Schoonheydt, R. A.; Mabbs, F. E.; Collison, D. *J. Chem. Soc., Faraday Trans.* **1996**, *92*, 2431.
(48) Weckhuysen, B. M.; Wachs, I. E.; Schoonheydt, R. A. *Chem. Rev.* **1996**, *96*, 3327.
(49) Zhu, Z.; Wasowicz, T.; Kevan, L. *J. Phys. Chem. B* **1997**, *101*, 10763.
(50) Rajic, N.; Stojakovic, D.; Hocevar, S. Kaucic, V. *Zeolites* **1993**, *13*, 384.
(51) Eswaramoorthy, M.; Jebarathinam, N. J.; Ulagappan, N.; Krishnasamy, V. *Catal. Lett.* **1996**, *38*, 255.
(52) Chapus, T.; Tuel, A.; Ben Taarit, Y.; Naccache, C. *Zeolites* **1994**, *14*, 349.
(53) Spinacé, E. V.; Cardoso, D.; Schuchardt, U. *Zeolites* **1997**, *19*, 6.
(54) Chen, J. D.; Sheldon, R. A. *J. Catal.* **1995**, *153*, 1.
(55) Peeters, M. P. J.; van de Ven, L. J. M.; de Haan, J. W.; van Hooff, J. H. C. *Colloids Surf. A* **1993**, *72*, 87.
(56) Kornatowski, J.; Finger, G.; Jancke, K.; Richter-Mendau, J.; Schultze, D.; Joswig, W.; Baur, W. H. *J. Chem. Soc., Faraday Trans.* **1994**, *90*, 2141.
(57) Goldfarb, D. *Zeolites* **1989**, *9*, 509.
(58) Levi, Z.; Raitsimring, A.; Goldfarb, D. *J. Phys. Chem.* **1991**, *95*, 7830.
(59) Brouet, G.; Chen, X.; Kevan, L. *J. Phys. Chem.* **1991**, *95*, 4928.

(60) Brouet, G.; Chen, X.; Lee, C. W.; Kevan, L. *J. Am. Chem. Soc.* **1992**, *114*, 3720.
(61) Lee, C. W.; Chen, X.; Brouet, G.; Kevan, L. *J. Phys. Chem.* **1992**, *96*, 3110.
(62) Brouet, G.; Chen, X.; Kevan, L. In *Proceedings of the 9th International Zeolite Conference, Montreal 1992*; von Ballmoos, R., Higgins, J. B., Treacy, M. M. J., Eds.; Butterworth-Heinemann: Stoneham, MA, 1993; p 489.
(63) Katzmarzyk, A.; Ernst, S.; Weitkamp, J.; Knözinger, H. *Catal. Lett.* **1991**, *9*, 85.
(64) Pluth, J. J.; Smith, J. V.; Richardson, W. R., Jr., *J. Phys. Chem.* **1988**, *92*, 2734.
(65) Akolekar, D.; Howe, R. F. In *Progress in Zeolite and Microporous Materials*; Studies in Surface Science and Catalysis; Chon, H., Ihm, S.-K., Uh, Y. S., Eds.; Elsevier: Amsterdam, 1996; Vol. 105, p 755.
(66) Batista, J.; Kaucic, V.; Hocevar, S. *Aust. J. Chem.* **1993**, *46*, 171.
(67) Olender, Z.; Goldfarb, D.; Batista, J. *J. Am. Chem. Soc.* **1993**, *115*, 1106.
(68) Chakrabarty, D. K.; Ashtekar, S.; Prakash, A. M.; Chilukuri, S. V. V. In *Progress in Zeolite and Microporous Materials*; Studies in Surface Science and Catalysis; Chon, H., Ihm, S.-K., Uh, Y. S., Eds.; Elsevier: Amsterdam, 1996; Vol. 105, p 517.
(69) Zubowa, H. L.; Richer, M.; Roost, U.; Parlitz, B.; Fricke, R. *Catal. Lett.* **1993**, *19*, 67.
(70) Catana, G.; Pelgrims, J.; Schoonheydt, R. A. *Zeolites* **1995**, *15*, 475.
(71) Park, J. W.; Chon, H. *J. Catal.* **1992**, *133*, 159.
(72) Hoppe, R.; Schulz-Ekloff, G.; Wohlrab, S.; Wöhrle, D. *Chem. Ing. Technol.* **1995**, *67*, 350.
(73) Goldfarb, D.; Bernardo, M.; Strohmaier, K. G.; Vaughan, D. E. W.; Thomann, H. *J. Am. Chem. Soc.* **1994**, *116*, 6344.
(74) Prasad, S.; Shinde, R. F.; Balakrishnan, I. *Microporous Mater.* **1994**, *2*, 159.
(75) Das, J.; Satyanaryana, V. V.; Chakrabarty, D. K.; Piramanayagam, S. N.; Shringi, S. N. *J. Chem. Soc., Faraday Trans.* **1992**, 88, 3255.
(76) Cardile, E. M.; Tapp, N. J.; Milestone, N. B. *Zeolites* **1990**, *10*, 90.
(77) Li, H. X.; Martens, J. A.; Jacobs, P. A.; Schubert, S.; Schmidt, F.; Zeithen, H. M.; Trautwein, A. X. In *Innovation in Zeolite Material Science*; Studies in Surface Science and Catalysis; Grobet, P. J., Mortier, W. J., Vansant, E. F., Schulz-Ekloff, G., Eds.; Elsevier: Amsterdam, 1988; Vol. 37, p 75.
(78) Ma, J.; Fan, B.; Li, R.; Cao, J. *Catal. Lett.* **1994**, *23*, 189.
(79) Iton, L. E.; Beal, R. B.; Hodul, D. T. *J. Mol. Catal.* **1983**, *21*, 151.
(80) Lin, D. H.; Coudurier, G.; Vedrine, J. C. In *Zeolites, Facts, Figures, Future*; Studies in Surface Science and Catalysis; Jacobs, P. A., van Santen, R. A., Eds.; Elsevier: Amsterdam, 1989; Vol. 49, p 227.
(81) Lund, A.; Nicholson, D. G.; Parish, R. V.; Wright, J. P. *Acta Chem. Scan.* **1994**, *48*, 738.
(82) Batista, J.; Kaucic, V.; Rajic, N.; Stojakovic, D. *Zeolites* **1992**, *12*, 925.
(83) Hill, S. J.; Williams, C. D.; Duke, C. V. A. *Zeolites* **1996**, *17*, 291.
(84) Canesson, L.; Tuel, A. *Zeolites* **1997**, *18*, 260.
(85) Duke, C. V. A.; Hill, S. J.; Williams, C. D. *J. Chem. Soc., Chem. Commun.* **1994**, 2633.
(86) Singh; P. S.; Shaikh, R. A.; Bandyopadhyay, R.; Rao, B. S. *J. Chem. Soc., Chem. Commun.* **1995**, 2255.
(87) Ahn, S.; Chon, H. *Microporous Mater.* **1997**, *8*, 113.
(88) Girnus, I.; Hoffmann, K.; Marlow, F.; Caro, J.; Döring, G. *Microporous Mater.* **1994**, *2*, 537.
(89) Yokomori, Y.; Kawachi, Y. *Zeolites* **1995**, *15*, 637.
(90) Ernst, S.; Puppe, L.; Weitkamp, J. In *Zeolites, Facts, Figures, Future*; Studies in Surface Science and Catalysis; Jacobs, P. A., van Santen, R. A., Eds.; Elsevier Science Publishers: Amsterdam, 1989; Vol. 49, p 447.
(91) Meusinger, J.; Vinek, H.; Lercher, J. *J. Mol. Catal.* **1994**, *87*, 263.
(92) Marchese, L.; Chen, J.; Thomas, J. M.; Coluccia, S.; Zecchina, A. *J. Phys. Chem.* **1994**, *98*, 13350.
(93) Montes, C.; Davis, M. E.; Murray, B. Narayana, M. *J. Phys. Chem.* **1990**, *94*, 6425.
(94) Prakash, A. M.; Hartmann, M.; Kevan, L. *J. Phys. Chem. B* **1997**, *101*, 6819.
(95) Zhang, G.; Harris, T. V. *Physica B* **1995**, *208 & 209*, 697.
(96) Bennett, J. M.; Marcus, B. K. In *Innovation in Zeolite Materials Science*; Studies in Surface Science and Catalysis; Grobet, P. J., Mortier, W. J., Vansant, E. F., Schulz-Ekloff, G., Eds.; Elsevier: Amsterdam, 1988; Vol. 37, p 269.
(97) Akolekar, D. P. *Catal. Lett.* **1994**, *28*, 249.
(98) Ashtekar, S.; Chilukuri, S. V. V.; Prakash, A. M.; Harendranath, C. S.; Chakrobarty, D. K. *J. Phys. Chem.* **1995**, *99*, 6937.
(99) Prakash, A. M.; Rao, K. V.; Unnikrishnan, S. *Ind. J. Chem. A* **1993**, *32*, 947.
(100) Iton, L. E.; Choi, I.; Desjardin, J. A.; Maroni, V. A. *Zeolites* **1989**, *9*, 535.
(101) Xu, R.; Maddox, P. J.; Couves, J. W. *J. Chem. Soc., Faraday Trans.* **1990**, *86*, 425.
(102) Kurshev, V.; Kevan, L.; Parillo, D. J.; Pereira, C.; Kokotailo, G. T.; Gorte, R. J. *J. Phys. Chem.* **1994**, *98*, 10160.
(103) Kurshev, V.; Kevan, L.; Parillo, D. J.; Gorte, R. J. In *Zeolite Science 1994: Recent Progress and Discussions*; Studies in Surface Science and Catalysis; Karge, H. G., Weitkamp, J., Eds.; Elsevier Science Publishers: Amsterdam, 1995; Vol. 98, p 79.
(104) Lohse, U.; Bertram, R.; Jancke, L.; Kurzawski, I.; Parlitz, B.; Löffler, E.; Schreier, E. *J. Chem. Soc., Faraday Trans.* **1995**, *91*, 1163.
(105) Berndt, H.; Martin, A.; Zhang, Y. *Microporous Mater.* **1996**, *6*, 1.
(106) Canesson, L.; Tuel, A. *Chem. Commun.* **1997**, 241.
(107) Van Breukelen, H. F. W. J.; Kraaijveld, G. L. C.; van de Ven, L. J. M.; de Haan, J. W.; van Hooff, J. H. C. *Microporous Mater.* **1997**, *12*, 313.
(108) Barrie, P. J.; Smith, M. E.; Klinowski, J. *Chem. Phys. Lett.* **1991**, *180*, 6.
(109) Barrie, P. J.; Klinowski, J. *J. Phys. Chem.* **1989**, *93*, 5974.
(110) Lohse, U.; Parlitz, B.; Müller, D.; Schreier, E.; Bertram, R.; Fricke, R. *Microporous Mater.* **1997**, *12*, 39.
(111) Racocy, R. A.; Ernst, S.; Hartmann, M.; Traa, Y.; Weitkamp, J. *Catal. Today* **1999**, *48*, in press.
(112) Kraushaar-Czarnetzki, B.; Hoogervorst, W. G. M.; Andrea, R. R.; Emeis, C. A.; Stork, W. H. In *Zeolite Chemistry and Catalysis*; Studies of Surface Science and Catalysis; Jacobs, P. A., Jäger, N. I., Kubelková, L., Wichterlová, B., Eds.; Elsevier: Amsterdam, 1991; Vol. 69, p 231.
(113) Prakash, A. M.; Chilukuri, S. V. V.; Ashtekar, S.; Chakrabarty, D. K. *J. Chem. Soc., Faraday Trans.* **1996**, *92*, 1257.
(114) Prasad, S.; Balakrishnan, I. *Catal. Lett.* **1991**, *11*, 105.
(115) Chen, S. H.; Shau, S. P.; Chao, K. J. *J. Chem. Soc., Chem. Commun.* **1992**, 1504.
(116) Schoonheydt, R. A.; de Vos, R.; Pelgrims, J.; Leeman, H. In *Zeolites: Facts, Figures, Future*; Studies in Surface Science and Catalysis; Jacobs, P. A., van Santen, R. A., Eds.; Elsevier: Amsterdam, 1989; Vol. 49, p 559.
(117) Shiralkar, V. P.; Saldarriaga, C. H.; Perez, J. O.; Clearfield, A. *Zeolites* **1989**, *9*, 474.
(118) Barrett, P. A.; Sankar, G.; Catlow, C. R. A.; Thomas, J. M. *J. Phys. Chem.* **1996**, *100*, 8977.
(119) Sankar, G.; Thomas, J. M.; Chen, J.; Wright, P. A.; Barrett, P. A.; Catlow, C. R. A.; Greaves, G. N. *Nucl. Instrum. Method, Phys. Res. Sect.* **1995**, *97*, 37.
(120) Chao, K. J.; Sheu, S. P.; Sheu, H. S. *J. Chem. Soc., Faraday Trans.* **1992**, *88*, 2949.
(121) Wu, C. N.; Chao, K. J.; Chang, H.; Lee, L. J.; Naccache, C. *J. Chem. Soc., Faraday Trans.* **1997**, *93*, 3551.
(122) Nakashiro, K.; Ono, Y. *Bull. Chem. Soc. Jpn.* **1993**, *66*, 9.
(123) Uytterhoeven, M. G.; Schoonheydt, R. A. *Microporous Mater.* **1994**, *3*, 265.
(124) Verberckmoes, A. A.; Uytterhoeven, M. G.; Schoonheydt, R. A. *Zeolites* **1997**, *19*, 180.
(125) Kraushaar-Czarnetzki, B.; Hoogervorst, W. G. M.; Andrea, R. R.; Emeis, C. A.; Stork, W. H. J. *J. Chem. Soc., Faraday Trans.* **1991**, *87*, 891.
(126) Peeters, M. P. J.; van Hooff, J. H. C.; Sheldon, R. A.; Zholobenko, V. L.; Kustov, L. M.; Kazansky, V. B. in *Proceedings of the 9th International Zeolite Conference*; von Ballmoos, R., Higgins, J. B., Treacy, M. M. J., Eds.; Butterworth-Heinemann: Stoneham, MA, 1992; p 627.
(127) Marchese, L.; Chen, J.; Thomas, J. M.; Coluccia, S.; Zecchina, A. *J. Phys. Chem.* **1994**, *98*, 13350.
(128) Chen, J.; Thomas, J. M.; Sankar, G. *J. Chem. Soc., Faraday Trans.* **1994**, *90*, 3455.
(129) Marchese, L.; Martra, G.; Damiliano, N.; Coluccia, S.; Thomas, J. M. *Stud. Surface Sci. Catal.* **1996**, *101*, 861−870.
(130) Thomas, J. M.; Greaves, G. N.; Sankar, G.; Wright, P. A.; Chen, J.; Dent, A. J.; Marchese, L. *Angew. Chem.* **1994**, *106*, 1922.
(131) Marchese, L.; Gianotti, E.; Damilano, N.; Coluccia, S.; Thomas, J. M. *Catal. Lett.* **1996**, *37*, 107.
(132) Moen, A.; Nicholson, D. G., Rønning, M.; Lamble, G. M.; Lee, J. F.; Emerich, H. *J. Chem. Soc., Faraday Trans.* **1997**, *93*, 4071.
(133) Han, H. S.; Chon, H. *Microporous Mater.* **1994**, *3*, 331.
(134) Lee, Y. J.; Chon, H. *J. Chem. Soc., Faraday Trans.* **1996**, *92*, 3453.
(135) Rajic, N.; Stojakovic, D.; Kaucic, V. *Zeolites* **1991**, *11*, 612
(136) Azuma, N.; Lee, C. W.; Kevan, L. *Proc. Symp. Petrol. Chem.* **1993**, *38*, 538.
(137) Azuma, N.; Lee, C. W.; Zamadics, M.; Kevan, L. In *Zeolites and Related Microporous Materials: State of the Art 1994*; Studies in Surface Science and Catalysis; Weitkamp, J., Karge, H. G., Pfeiffer, H., Hölderich, W., Eds.; Elsevier: Amsterdam, 1994; Vol. 84, p 805.
(138) Azuma, N.; Lee, C. W.; Kevan, L. *J. Phys. Chem.* **1994**, *98*, 1217.
(139) Azuma, N.; Kevan, L. *J. Phys. Chem.* **1995**, *99*, 5083.
(140) Azuma, N.; Hartmann, M.; Kevan, L. *J. Phys. Chem.* **1995**, *99*, 6670.

(141) Che, M.; Richard, M.; Olivier, D. *J. Chem. Soc., Faraday Trans.* **1980**, *76*, 1526.
(142) Hartmann, M.; Azuma, N.; Kevan, L. *J. Phys. Chem.* **1995**, *99*, 10988.
(143) Hartmann, M.; Azuma, N.; Kevan, L. In *Zeolites: A Refined Tool for Designing Catalytic Sites*; Studies in Surface Science and Catalysis; Bonneviot, L., Kaliaguine, S., Eds.; Elsevier: Amsterdam, 1995; Vol. 97, p 335.
(144) Spojakina, A.; Kostova, N.; Penchev, V. In *Zeolite Science 1994: Recent Progress and Discussions*; Studies in Surface Science and Catalysis; Karge, H. G., Weitkamp, J., Eds.; Elsevier: Amsterdam, 1995; Vol. 98, p 75.
(145) Prakash, A. M.; Wasowicz, T.; Kevan, L. *J. Phys. Chem.* **1996**, *100*, 15947.
(146) Akolekar, D. B. *J. Mol. Catal. A* **1995**, *104*, 95.
(147) (a) Minchev, C.; Zubkov, S. A.; Valtchev, V.; Monkov, V.; Micheva, N.; Kanazirev, V. *Appl. Catal. A* **1994**, *119*, 195. (b) Spojakima, A.; Kostova, N.; Penchev, C. in: *Zeolite Science 1994: Recent Progress and Discussions*, Studies in Surface Science and Catalysis; Karge, H. G., Weitkamp, J., Eds.; Elsevier: Amsterdam, 1995; Vol. 98, p 75.
(148) Marrodinova, V.; Neinska, Y.; Minchev, C.; Lechert, H.; Minkov, V.; Valtchev, V.; Penchev, V. In *Zeolite Chemistry and Catalysis*; Studies of Surface Science and Catalysis; Jacobs, P. A., Jäger, N. I., Kubelková, L., Wichterlová, B., Eds.; Elsevier: Amsterdam, 1991; Vol. 69, p 295.
(149) Elangovan, S. P.; Krishnasamy, V.; Murugesan, V. *Bull. Chem. Soc. Jpn.* **1995**, *68*, 3659.
(150) Xu, R.; Maddox, P. J.; Thomas, J. M. *Polyhedron* **1989**, *8*, 819.
(151) Inui, T.; Phatanasrim, S. Matsuda, H. *J. Chem. Soc., Chem Commun.* **1990**, 205.
(152) Couves, J. W.; Sanakov, G.; Thomas, J. M.; Chen, J.; Catlow, C. R. A.; Xu, R.; Greaves, G.N. In *Proceedings of the 9th International Zeolite Conference, Montreal 1992*; von Ballmoos, R., Higgins, J. B., Treacy, M. M. J., Eds.; Butterworth-Heinemann: Stoneham, MA, 1993; p 627.
(153) Duke, C. V. A.; Hill, S. J.; Williams, C. D. *Zeolites* **1995**, *15*, 413.
(154) Prakash, A. M.; Hartmann, M.; Kevan, L. *J. Chem. Soc., Faraday Trans.* **1997**, *93*, 1233.
(155) Zholobenko, V.; Garforth, A.; Clark, L.; Dwyer, J. In *Zeolites a Refined Tool for Designing Catalytic Sites*; Studies in Surface Science and Catalysis; Bonneviot, L., Kaliaguine, S., Eds.; Elsevier: Amsterdam, 1995; Vol. 97, p 395.
(156) Lee, C. W.; Yu, J. S.; Kevan, L. *J. Phys. Chem.* **1992**, *96*, 7747.
(157) Saint-Pierre, T.; Chen, X.; Kevan, L. *J. Phys. Chem.* **1993**, *97*, 932.
(158) Yu, J. S.; Comets, J. M.; Kevan, L. *J. Phys. Chem.* **1993**, *97*, 10433.
(159) Yu, J. S.; Lee, C. W.; Kevan, L. *J. Phys. Chem.* **1994**, *98*, 5741.
(160) Yu, J. S.; Kurshev, V. Kevan, L. *J. Phys. Chem.* **1994**, *98*, 10225.
(161) (a) Back, G. H.; Yu, J. S.; Kurshev, V.; Kevan, L. *J. Chem. Soc., Faraday Trans.* **1994**, *90*, 2283. (b) Yu, J. S.; Back, G. H.; Kurshev, V. Kevan, L. In *Zeolite Science 1994: Recent Progress and Discussions*; Studies in Surface Science and Catalysis; Karge, H. G., Weitkamp, J., Eds.; Elsevier: Amsterdam, 1995; Vol. 98, p 77.
(162) Kevan, L. *Rev. Chem. Int.* **1987**, *8*, 53.
(163) Ishihara, T.; Sumi, H.; Takita, Y. *Chem. Lett.* **1994**, 1499.
(164) Parlitz, B.; Schreier, E.; Zubowa, H. L.; Eckelt, R.; Lieske, E.; Lischke, G.; Fricke, R. *J. Catal.* **1995**, *155*, 1.
(165) Chen, X.; Kevan, L. *J. Am. Chem. Soc.* **1991**, *113*, 2861.
(166) Lee, C. W.; Chen, X.; Kevan, L. *Catal. Lett.* **1992**, *15*, 75.
(167) Lee, C. W.; Chen, X.; Kevan, L. *J. Phys. Chem.* **1992**, *96*, 357.
(168) Lee, C. W.; Brouet, G.; Chen, X.; Kevan, L. *Zeolites* **1993**, *13*, 565.
(169) Lee, C. W.; Kevan, L. *Zeolites* **1994**, *14*, 267.
(170) Vansant, E. F.; Lunsford, J. H. *J. Phys. Chem.* **1972**, *76*, 2860.
(171) Rajic, N.; Stojakovic, D.; Kaucic, V. *Zeolites* **1991**, *11*, 612.
(172) Moen, A.; Nicholson, D. G. *J. Chem. Soc., Faraday Trans.* **1995**, *91*, 3529.
(173) Munoz, T.; Prakash, A. M.; Kevan, L.; Balkus, K. J. *J. Phys. Chem. B* **1998**, *102*, 1379.
(174) (a) Zamadics, M.; Chen, X.; Kevan, L. *J. Phys. Chem.* **1992**, *96*, 2652. (b) Zamadics, M.; Chen, X.; Kevan, L. *J. Phys. Chem.* **1992**, *96*, 5488.
(175) Pluth, J. J.; Smith, J. V.; Mortier, W. J. *Mater. Res. Bull.* **1979**, *2*,1001.
(176) Zamadics, M.; Kevan, L. *J. Phys. Chem.* **1992**, *96*, 8989.
(177) Lee, C. W.; Chen, X.; Zamadics, M.; Kevan, L. *J. Chem. Soc., Faraday Trans.* **1993**, *89*, 4137.
(178) Zamadics, M.; Kevan, L. *J. Phys. Chem.* **1993**, *97*, 10102.
(179) Zamadics, M.; Kevan, L. *J. Phys. Chem.* **1992**, *96*, 1041.
(180) Zamadics, M.; Kevan, L. *J. Phys. Chem.* **1993**, *97*, 3359.
(181) Anderson, M. W.; Kevan, L. *J. Phys. Chem.* **1986**, *90*, 3206.
(182) Wasowicz, T.; Kim, S. J.; Hong, S. B.; Kevan, L. *J. Phys. Chem.* **1996**, *100*, 15954.
(183) Prakash, A. M.; Kevan, L. *Langmuir* **1997**, *13*, 5341.
(184) Hartmann, M.; Kevan, L. *J. Chem. Soc., Faraday Trans.* **1996**, *92*, 3661.
(185) Whittington, B. I.; Anderson, J. R. *Catal. Lett.* **1992**, *16*, 1.
(186) Panayotov, D.; Dimitrov, L.; Khristova, M.; Petrov, L.; Mehandjiev, D. *Appl. Catal. B* **1995**, *6*, 61.
(187) Ishihara, T.; Kagawa, M.; Mizuhara, Y.; Takita, Y. *Chem. Lett.* **1992**, 2119.
(188) Lechert, H.; Weyda, H.; Hess, M.; Kleinworth, R.; Penchev, V.; Minchev, Ch. In *Zeolite Chemistry and Catalysis*; Studies of Surface Science and Catalysis; Jacobs, P. A., Jäger, N. I., Kubelková, L., Wichterlová, B., Eds.; Elsevier: Amsterdam, 1991; Vol. 69, p 145.
(189) Roque-Malherbe, R.; Lopez-Cordero, R.; Gonzales-Morales, J. A.; Onate-Martinez, J.; Carreras-Gracial, M. *Zeolites* **1993**, *13*, 481.
(190) Lourenco, J. P.; Ribeiro, M. F.; Ramoa Ribeiro, F.; Rocha, J.; Onida, J.; Garrone, E.; Gabelica, Z. *Zeolites* **1997**, *18*, 398.
(191) Novak Tusar, N.; Meden, A.; Arcon, I.; Kodre, A.; Kaucic, V. In *Catalysis by Microporous Materials*; Studies in Surface Science and Catalysis; Beyer, H. K., Karge, H. G., Kiricsi, I., Nagy, J. B., Eds.; Elsevier: Amsterdam, 1995; Vol. 94, p 232.
(192) Novak Tusar, N.; Kaucic, V.; Geremia, S.; Vlaic, G. *Zeolites* **1995**, *15*, 708.
(193) Chen, J.; Thomas, J. M.; Sankar, G. *J. Chem. Soc., Faraday Trans.* **1994**, *90*, 3455.
(194) Hocevar, S.; Batista, J.; Kaucic, V. *J. Catal.* **1993**, *139*, 351.
(195) Tuel, A.; Arcon, I.; Noval Tusar, N.; Meden, A.; Kaucic, V. *Microporous Mater.* **1996**, *7*, 271.
(196) Elangovan, S. P.; Krishnasamy, V.; Murugesan, V. *Catal. Lett.* **1996**, *36*, 271.
(197) Akolekar, D. B. *Appl. Catal.* **1994**, *112*, 125.
(198) Escalante, D.; Méndez, B.; Hernández, G.; López, C. M.; Machado, F. J.; Goldwasser, J.; Ramirez de Agudelo, M. M. *Catal. Lett.* **1997**, *47*, 229.
(199) Gielgens, L. H.; Veenstra, I. H. E.; Ponec, V.; Haanepen, M. J.; van Hooff, J. H. C. *Catal. Lett.* **1995**, *32*, 195.
(200) Sierra, L.; Patarin, J.; Guth, J. L. *Microporous Mater.* **1997**, *11*, 19.
(201) Huang, M.; Yao, J.; Xu, S.; Meng, C. *Zeolites* **1992**, *12*, 810.
(202) Lee, C. W.; Saint-Pierre, T.; Azuma, N.; Kevan, L. *J. Phys. Chem.* **1993**, *97*, 11811.
(203) Campelo, J. M.; Lafont, F.; Marinas, J. M. *J. Chem. Soc., Faraday Trans.* **1995**, *91*, 1551.
(204) Campelo, J. M.; Lafont, F.; Marinas, J. M. *Zeolites* **1995**, *15*, 97.
(205) Campelo, J. M.; Lafont, F.; Marinas, J. M. *Appl. Catal. A* **1997**, *152*, 53.
(206) Chaar, M. A.; Butt, J. B. *Appl. Catal. A* **1994**, *114*, 287.
(207) Campelo, J. M.; Lafont, F.; Marinas, J. M. *J. Chem. Soc., Faraday Trans.* **1995**, *91*, 4171.
(208) Hoffmeister, M.; Butt, J. B. *Appl. Catal. A* **1992**, *82*, 169.
(209) Mériaudeau, P.; Tuan, V. A.; Nghiem, V. T.; Lai, S. Y.; Hung, L. N.; Naccache, C. *J. Catal.* **1997**, *169*, 55.
(210) Miller, S. J. *Microporous Mater.* **1994**, *2*, 439.
(211) Blackmond, D. G.; Swid, K. P.; Davis, M. E.; Gallezot, P. *J. Catal.* **1990**, *122*, 247.
(212) Michalik, J.; Azuma, N.; Sadlo, J.; Kevan, L. *J. Phys. Chem.* **1995**, *99*, 9, 4679.
(213) Michalik, J.; Van der Pol, A.; Reijerse, E. J.; Wasowicz, T.; de Boer, E. *Appl. Magn. Res.* **1992**, *3*, 19.
(214) Michalik, J.; Zamadics, M.; Sadlo, J.; Kevan, L. *J. Phys. Chem.* **1993**, *97*, 10440.
(215) Michalik, J.; Zamadics, M.; Sadlo, J.; Kevan, L. In *Zeolites and Related Microporous Materials: State of the Art 1994*; Studies in Surface Science and Catalysis; Weitkamp, J., Karge, H. G., Pfeiffer, H., Hölderich, W., Eds.; Elsevier: Amsterdam, 1994, Vol. 84, p 957.
(216) Michalik, J.; Kevan, L. *J. Am. Chem. Soc.* **1991**, *113*, 2861.
(217) Mériaudeau, P.; Tuan, V. A.; Hung, L. N.; Lefebvre, F.; Nguyen, H. P. *J. Chem. Soc., Faraday Trans.* **1997**, *93*, 4201.
(218) Hartmann, M.; Kevan, L. *J. Chem. Soc., Faraday Trans.* **1996**, *92*, 1429.
(219) Hartmann, M.; Kevan, L. In *Progress in Zeolite and Microporous Materials*; Studies in Surface Science and Catalysis; Chon, H., Ihm, S.-K., Uh, Y. S., Eds.; Elsevier: Amsterdam, 1996; Vol. 105, p 717.
(220) Hartmann, M.; Kevan, L. *J. Phys. Chem.* **1996**, *100*, 4606.
(221) Alex, A.; Clark, T. *J. Am. Chem. Soc.* **1992**, *114*, 506.
(222) Jacobs, P. A.; Declerck, D. J.; Vandamme, L. J.; Uytterhoeven, J. B. *J. Chem. Soc., Faraday Trans. 1* **1975**, *71*, 1545.
(223) Sheldon, R. A.; de Heij, N. In *The Role of Oxygen in Chemistry and Biochemistry*; Ando, W., Mora-oka, Y., Eds.; Elsevier: Amsterdam, 1988; p 243.
(224) Dakka, J.; Sheldon, R. A. Netherlands Pat. 9200968, 1992.
(225) Lin, S. S.; Weng, H. S. *Appl. Catal. A* **1993**, *105*, 289.
(226) Vanoppen, D. L.; De Vos, D. E.; Genet, M. J.; Rouxhet, P. G.; Jacobs, P. A. *Angew. Chem.* **1995**, *107*, 637.
(227) Lin, S. S.; Weng, H. S. *J. Chem. Eng. Jpn.* **1994**, *27*, 211.
(228) Sheldon, R. A.; Chen, J. D.; Dakka, J.; Neelemam, E. *Preprints of the 1st World Congress on Selective Oxidation*; Belmaneda, Spain, 1992; paper G1.
(229) Chen, J. D.; Dakka, J.; Neeleman, E.; Sheldon, R. A. *J. Chem. Soc., Chem. Commun.* **1993**, 1379.

(230) Dakka, J.; Sheldon, R. A. *Appl. Catal. A* **1994**, *108*, L1.
(231) Haanepen, M. J.; van Hoff, J. H. C. In *Tagungsbericht 9204, Proceedings of the GMF Conference on Selective Oxidations in Petrochemistry*; Goslar, Germany, 1992; p 227.
(232) (a) Haanepen, M. J.; van Hooff, J. H. C. *Appl. Catal.* **1997**, *152*, 183. (b) Haanepen, M. J.; Elemans-Mehring, A. M.; van Hooff, J. H. C. *Appl. Catl.* **1997**, *152*, 203.
(233) Dai, P. S. E.; Petty, R. H.; Ingram, C. W.; Szostak, R. *Appl. Catal. A* **1996**, *143*, 101.
(234) Concepcion, P.; López Nieto, J. M.; Pérez-Pariente, J. *Catal. Lett.* **1993**, *19*, 333.
(235) Concepcion, P.; López Nieto, J. M.; Pérez-Pariente, J. *Catal. Lett.* **1994**, *28*, 9.
(236) Concepcion, P.; López Nieto, J. M.; Pérez-Pariente, J. *J. Mol. Catal.***1995**, *99*, 173.
(237) Wan, B. Z.; Huang, K. *Appl. Cata.* **1991**, *73*×e2 113.
(238) Concepción, P.; Corma, A.; López Nieto, J. M.; Pérez-Pariente, J. *Appl. Catal. A* **1996**, *143*, 17.
(239) Huybrechts, D. R. C.; Buskens, P. L.; Jacobs, P. A. *J. Mol. Catal.* **1992**, *71*, 129.
(240) Inui, T.; Matsuda, H.; Okaniwa, H.; Miyamoto, A. *Appl. Catal.* **1990**, 58, 155.
(241) Chen, J.; Wright, P. A.; Thomas, J. M.; Natarajan, S.; Marchese, L.; Bradley, S. M.; Sankar, G.; Catlow, C. R. A.; Gai-Boyes, P. L.; Townsend, R. A.; Lok, C. M. *J. Phys. Chem.* **1994**, *98*, 10216.
(242) Inui, T.; Phatanasri, S.; Matsuda, H. *J. Chem. Soc., Chem. Commun.* **1990**, 205.
(243) Thomas, J. M.; Xu, Y.; Catlow, C. R. A.; Couves, J. W. *Chem. Mater.* **1991**, *3*, 667.
(244) Hocevar, S.; Levec, J. *J. Catal.* **1992**, *135*, 518.
(245) Chen, J.; Thomas, J. M. *J. Chem. Soc., Chem. Commun.* **1994**, 603.
(246) Wendelbo, R.; Akporiaye, Andersen, A.; Dahl, I. M.; Mostad, H. B. *Appl. Catal. A* **1996**, *142*, L197.
(247) Smith, L.; Cheetham, A. K.; Marchese, L.; Thomas, J. M.; Wright, P. A.; Chen, J.; Gianotti, E. *Catal. Lett.* **1996**, *41*, 13.
(248) Chen, J.; Wright, P. A.; Natarajan, S.; Thomas, J. M. In *Zeolites and Related Microporous Materials: State of the Art 1994*; Studies in Surface Science and Catalysis; Weitkamp, J., Karge, H. G., Pfeiffer, H., Hölderich, W., Eds.; Elsevier: Amsterdam, 1994, Vol. 84, p 1731.
(249) Hocevar, S.; Batista, J.; Kaucic, V. *J. Catal.* **1993**, *139*, 351.
(250) Rajic, N.; Stojakovic, D.; Hocevar, S.; Kaucic, V. *Zeolites* **1993**, *13*, 384.
(251) Lischke, G.; Parlitz, B.; Lohse, U.; Schreier, E.; Fricke, R. *Appl. Catal. A* **1998**, *166*, 351.
(252) Balkus, K. J., Jr.; Ball, L. J.; Gimon-Kinsel, M. E.; Anthony, J. M.; Gnade, B. E. *Sens. Actuators B* **1997**, *42*, 67.
(253) Schulz-Ekloff, G. In *Advanced Zeolite Science and Applications*; Studies in Surface Science and Catalysis; Jansen, J. C., Stöcker, M., Karge, H. G., Weitkamp, J., Eds.; Elsevier: Amsterdam, 1994; Vol. 85, p 145.
(254) Centi, G.; Perathorer, S.; Trifiro, F.; Aboukais, A.; Aissi, C. F.; Guelton, M. *J. Phys. Chem.* **1992**, *96*, 2617.
(255) Sass, C. E.; Chen, X.; Kevan, L. *J. Chem. Soc., Faraday Trans.* **1990**, *86*, 189.
(256) Fejes, P.; Marsi, I.; Kiricsi, I.; Halasz, J.; Hannus, J.; Rockenbauer, A.; Tasi, G.; Korecz, L.; Schöbel, G. In *Zeolite Chemistry and Catalysis*; Studies of Surface Science and Catalysis; Jacobs, P. A., Jäger, N. I., Kubelková, L., Wichterlová, B., Eds.; Elsevier: Amsterdam, 1991; Vol. 69, p 173.
(257) DiGrejorio, S.; Greenblatt, M.; Pifer, J. H.; Sturge, M. D. *J. Chem. Phys.* **1982**, *76*, 2931.
(258) Kulkarni, S. J.; Ramachandra Rao, R.; Subrahmanyam, M.; Rama, Rao, A. V.; Sarkany, A.; Guczi, L. *Appl. Catal. A* **1996**, *139*, 59.
(259) Luan, Z.; Xu, J.; He, H.; Klinowski, J.; Kevan, L. *J. Phys. Chem.* **1996**, *100*, 19595.
(260) Sheldon, R. A.; Wallau, M.; Arends, I. W. C. E.; Schuchardt, U. *Acct. Chem. Res.* **1998**, *31*, 485.

CR9600971